

NAVAL POSTGRADUATE SCHOOL

Monterey, California



THESIS

SWELL TRANSFORMATION ACROSS THE CONTINENTAL SHELF

by

Cynthia Viernes Tinder

June 2000

Thesis Advisor:
Second Reader:

Thomas H.C. Herbers
Edward B. Thornton

Approved for public release; distribution is unlimited.

THIS QUANTITY INSPECTED 4

20000818 062

REPORT DOCUMENTATION PAGE			Form Approved OMB No. 0704-0188	
Public reporting burden for this collection of information is estimated to average 1 hour per response, including the time for reviewing instruction, searching existing data sources, gathering and maintaining the data needed, and completing and reviewing the collection of information. Send comments regarding this burden estimate or any other aspect of this collection of information, including suggestions for reducing this burden, to Washington headquarters Services, Directorate for Information Operations and Reports, 1215 Jefferson Davis Highway, Suite 1204, Arlington, VA 22202-4302, and to the Office of Management and Budget, Paperwork Reduction Project (0704-0188) Washington DC 20503.				
1. AGENCY USE ONLY (Leave blank)		2. REPORT DATE June 2000	3. REPORT TYPE AND DATES COVERED Master's Thesis	
TITLE AND SUBTITLE : Swell Transformation Across the Continental Shelf			5. FUNDING NUMBERS	
6. AUTHOR(S) Cynthia Viernes Tinder				
7. PERFORMING ORGANIZATION NAME(S) AND ADDRESS(ES) Naval Postgraduate School Monterey, CA 93943-5000			8. PERFORMING ORGANIZATION REPORT NUMBER	
9. SPONSORING / MONITORING AGENCY NAME(S) AND ADDRESS(ES) N/A			10. SPONSORING / MONITORING AGENCY REPORT NUMBER	
11. SUPPLEMENTARY NOTES The views expressed in this thesis are those of the author and do not reflect the official policy or position of the Department of Defense or the U.S. Government.				
12a. DISTRIBUTION / AVAILABILITY STATEMENT Approved for public release; distribution is unlimited			12b. DISTRIBUTION CODE	
ABSTRACT (maximum 200 words) A preliminary analysis of swell decay across the continental shelf was conducted using data from the SHOaling Waves EXperiment (SHOWEX). Six Datawell Directional Waverider buoys were deployed along a cross-shelf transect, offshore of Duck, North Carolina during an active hurricane season in the fall of 1999. Estimates of the frequency spectrum, $E(f)$, mean propagation direction, $\theta_{mean}(f)$, and directional spread, $\sigma_\theta(f)$, were obtained from the auto-, co- and quadrature spectra of the horizontal and vertical orbital displacements measured by the buoys. Twelve cases were analyzed including eight cases dominated by remotely generated long period swells arriving from various directions. The last four cases were characterized by active wave generation by strong winds on the continental shelf, including the passages of Hurricanes Floyd and Irene. Comparisons of significant wave heights of swell observed at all buoys show a consistent strong decay across the shelf supporting the major role of bottom friction in swell transformation. A decline in wave heights near the coast was also observed during the passage of hurricanes, due to limited fetch and enhanced bottom friction in shallow water. Estimates of θ_{mean} show the expected refraction of waves to shore-normal directions on the inner shelf. Estimates of σ_θ generally do not vary much across the shelf. However, a sharp increase of σ_θ across the inner shelf was observed for directionally narrow swells from Hurricane Gert, possibly due to wave scattering from bottom irregularities. In all cases, σ_θ was at a minimum at the spectral peak frequency.				
14. SUBJECT TERMS Swell Transformation, Continental Shelf, Directional Wave Spectra, Wave Dissipation, Wave Buoy, Refraction			15. NUMBER OF PAGES 72	
			16. PRICE CODE	
17. SECURITY CLASSIFICATION OF REPORT Unclassified	18. SECURITY CLASSIFICATION OF THIS PAGE Unclassified	19. SECURITY CLASSIFICATION OF ABSTRACT Unclassified	20. LIMITATION OF ABSTRACT UL	

THIS PAGE INTENTIONALLY LEFT BLANK

Approved for public release; distribution is unlimited

SWELL TRANSFORMATION ACROSS THE CONTINENTAL SHELF

Cynthia Viernes Tinder
Lieutenant, United States Navy
B.S., United States Naval Academy, 1993

Submitted in partial fulfillment of the
requirements for the degree of

**MASTER OF SCIENCE IN METEOROLOGY AND PHYSICAL
OCEANOGRAPHY**

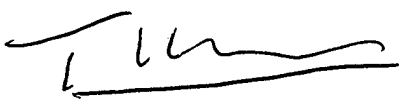
from the

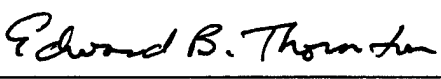
**NAVAL POSTGRADUATE SCHOOL
June 2000**

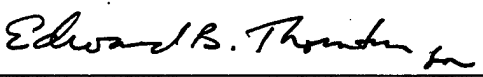
Author:


Cynthia Viernes Tinder

Approved by:


Thomas H.C. Herbers, Thesis Advisor


Edward B. Thornton, Second Reader


Roland W. Garwood, Jr., Chairman
Department of Oceanography

THIS PAGE INTENTIONALLY LEFT BLANK

ABSTRACT

A preliminary analysis of swell decay across the continental shelf was conducted using data from the SHOaling Waves EXperiment (SHOWEX). Six Datawell Directional Waverider buoys were deployed along a cross-shelf transect, offshore of Duck, North Carolina during an active hurricane season in the fall of 1999. Estimates of the frequency spectrum, $E(f)$, mean propagation direction, $\theta_{mean}(f)$, and directional spread, $\sigma_{\theta}(f)$, were obtained from the auto-, co- and quadrature spectra of the horizontal and vertical orbital displacements measured by the buoys. Twelve cases were analyzed including eight cases dominated by remotely generated long period swells arriving from various directions. The last four cases were characterized by active wave generation by strong winds on the continental shelf, including the passages of Hurricanes Floyd and Irene. Comparisons of significant wave heights of swell observed at all buoys show a consistent strong decay across the shelf supporting the major role of bottom friction in swell transformation. A decline in wave heights near the coast was also observed during the passage of hurricanes, due to limited fetch and enhanced bottom friction in shallow water. Estimates of θ_{mean} show the expected refraction of waves to shore-normal directions on the inner shelf. Estimates of σ_{θ} generally do not vary much across the shelf. However, a sharp increase of σ_{θ} across the inner shelf was observed for directionally narrow swells from Hurricane Gert, possibly due to wave scattering from bottom irregularities. In all cases, σ_{θ} was at a minimum at the spectral peak frequency.

THIS PAGE INTENTIONALLY LEFT BLANK

TABLE OF CONTENTS

I. INTRODUCTION.....	1
II. FIELD EXPERIMENT.....	7
III. DATA ANALYSIS.....	11
IV. CASE STUDIES.....	17
V. CROSS-SHELF VARIATIONS.....	23
A. EASTERLY SWELLS.....	23
B. LARGE OBLIQUE ANGLE SWELLS.....	24
C. STORM WAVES.....	25
VI. FREQUENCY DIRECTIONAL SPECTRA.....	27
VII. CONCLUSIONS.....	33
APPENDIX. FIGURES.....	35
LIST OF REFERENCES.....	55
INITIAL DISTRIBUTION LIST.....	57

ACKNOWLEDGEMENTS

This research was funded by the Office of Naval Research. The field experiment was conducted in collaboration with Dr. William C. O'Reilly (Scripps Institute of Oceanography). The tireless efforts of Paul Jessen, Fabrice Ardhuin, Dr. Thomas H. C. Herbers, the staff of the Scripps Institute of Oceanography Center of Coastal Studies and the crew of the R/V Cape Hatteras during the deployment and recovery of the six Datawell Directional Waverider buoys are greatly appreciated. Permission to use these data is appreciated.

Heartfelt gratitude is extended to my advisor, Dr. Thomas H.C. Herbers, for his guidance, patience, and instruction during my pursuit of this study. Sincere gratitude is extended to Paul Jessen, for providing dedicated technical assistance in maintaining the buoys during deployment and persevering during the worst weather. His assistance in matlab programming and creating the base for several figures in this study is greatly appreciated. My family and friends gave tremendous support and encouragement.

I. INTRODUCTION

Swell characteristics transform dramatically between the open ocean and the beach. When the water depth becomes comparable to the swell wavelength, the bottom starts to influence swell propagation by causing changes in the wave phase and group speeds.

As swells begin to shoal the group speed initially increases, and it follows from the conservation of energy that the wave amplitude decreases by as much as 10% in intermediate water depths ($kh \approx 1$, where k is the wave number and h is the water depth). In shallower water, the group speed decreases with decreasing depth, causing an increase in wave amplitudes near the coast.

The phase speed changes associated with depth variations cause refraction analogous to Snell's law in geometric optics. Monochromatic wave trains propagating over a shelf with straight and parallel depth contours, refract such that the crests become more parallel to the beach. In situations with complex bathymetry, refraction can cause large wave height variations. Wave propagation directions generally refract towards shallower regions, typically causing a convergence region of larger waves near shoals, headlands and ridges, and divergence regions of smaller waves in bays and near submarine canyons (e.g., Munk and Traylor, 1947). Significant refraction effects occur as waves travel over a large submerged topographic feature, but also when waves move through a large shallow coastal region with smooth undulating topography (e.g., Graber et al., 1990; O'Reilly and Guza, 1993).

Shoaling and refraction are linear processes that are well understood theoretically. By applying an energy balance along ray trajectories, the evolution of wave spectra can be evaluated for arbitrary two-dimensional continental shelf topography (e.g., Munk and Arthur, 1951; Longuet-Higgins, 1957; Le Méhauté and Wang, 1982).

Although swell can cross entire ocean basins with minor energy losses (Snodgrass et al., 1966), significant dissipation of swell energy takes place on a shallow continental shelf. There are several mechanisms through which the bottom can remove energy from the waves and reduce wave heights. Shemdin et al. (1980) evaluated the relative importance of bottom friction (usually most dominant in sandy bottoms with 0.1-0.4 mm grain diameter), percolation through the bottom (coarser sediments with diameter ≥ 0.5 mm), and wave-induced bottom motion (fine sediment). The sediment type, bottom microtopography, in particular, the presence of ripples, and local currents play important roles in the damping rates, all of which are often unknown.

On the sandy continental shelf considered in this study, bottom friction is believed to be the dominant swell decay mechanism. Bottom friction is dependent on both sand ripple characteristics and the prevailing sea-state conditions at the site. Tolman (1994) reviewed the important feed back between ripple formation and wave energy dissipation. Orbital sand ripples, initiated when the orbital wave motion near the bottom is strong enough to move sediment, greatly enhance the bottom roughness (Grant and Madsen, 1982). Tolman's (1994) model of wave-generated bedforms and associated damping of swell across a continental shelf suggest that moderately energetic swell shoaling on a continental shelf can generate sand ripples that cause strong damping of the swell.

Few measurements of the attenuation of swell in shallow water have been reported. The JONSWAP experiment examined the swell decay observed over a 160-km-long cross-shore transect of various instruments deployed off the coast of Germany (Hasselmann et al., 1973). The observed damping rates did not agree with generally accepted formulations of bottom friction and suggested that other attenuation mechanisms such as back-scattering of swell from small scale bottom irregularities may be important (Long, 1973). Young and Gorman (1995) conducted a 2-week-long experiment using a cross-shore transect of various types of instruments spanning the continental shelf on the southern coast of Australia. These measurements were used in conjunction with the spectral wave model WAM (The WAMDI Group, 1988) to estimate the contribution of bottom friction to the observed overall decrease in swell energy across the shelf. The results suggested that the strong attenuation of energetic southern ocean swells observed at shallow instrument sites is primarily caused by bottom friction with estimated drag coefficients that are much larger than the values used in wave prediction models. Forristall and Reece (1985) measured wave attenuation and bottom processes near the Mississippi Delta in the Sea Wave Attenuation Measurement Program (SWAMP). They suspected that the soft bottom near river deltas causes strong swell attenuation. The observed attenuation was a strong function of the deep-water significant wave height and a weak function of the wave frequency. Refraction and shoaling accounted for the changes in the directional spectra when the wave height was small. With larger wave heights (> 3 m), significant attenuation was observed, in particular for frequencies < 0.10 Hz.

Herbers et al. (2000) studied the transformation of swell across the continental shelf off the coast of North Carolina. The results suggested that on the outer shelf energy was lost only by the lower frequencies of the spectrum, possibly because high-frequency components with relatively shorter wavelengths were unattenuated at the bottom. At the shallower sites, observed spectral levels were lower than predicted spectral levels at all frequencies, suggesting significant damping of all components of the spectrum. The apparent damping is strongest near the peak frequency causing a slight broadening of the observed spectrum at the closest nearshore site. The inferred friction factor agreed roughly with the results from Young and Gorman's study, and was much larger than those commonly used in wave prediction models (e.g., The WAMDI Group, 1988).

New observations of the evolution of swell across a continental shelf are presented here. Six Datawell Directional Waverider buoys were deployed along a 100 km cross-shelf transect off the coast of North Carolina for 3 months in 1999 as part of the SHOWEX (SHoaling Waves EXperiment). In contrast to previous experiments that provided estimates of swell height decay across the shelf, the detailed directional wave measurements collected in SHOWEX also allow for an analysis of the transformation of directional wave properties across the shelf. An unusually active hurricane season caused by La Niña conditions provided numerous case studies of energetic long period swell. The field experiment is described in Chapter II, followed by a description of the data analysis procedures in Chapter III. Twelve case studies are presented in Chapter IV, followed by an analysis of observed cross-shelf variations in Chapter V. Chapter VI

discusses the frequency-directional spectra, and the results are summarized in Chapter

VII.

THIS PAGE INTENTIONALLY LEFT BLANK

II. FIELD EXPERIMENT

The field data used in this study were collected as part of the ONR SHOaling Waves EXperiment (SHOWEX) conducted offshore of the U.S. Army Corps of Engineers Field Research Facility (FRF) near Duck, North Carolina, from mid-September to mid-December, 1999. The site is located about midway between Cape Hatteras and Chesapeake Bay, along a coast consisting of a series of relatively straight barrier islands with sandy beaches that are fully exposed to the Atlantic Ocean.

The continental shelf is oriented approximately north-south, and widens from Cape Hatteras toward Chesapeake Bay. The continental shelf is about 100 km wide and only 20 – 50 m deep across most of the study site (Figure 1). Bathymetry is characterized by a gently sloping inner shelf (about 1:250), extending into a wide mid-shelf region with an even lower slope of about 1:2500 and large ($O(5 \text{ km})$) ridge-like features that have vertical scales of $O(5 \text{ m})$. The continental shelf widens from Cape Hatteras, North Carolina, and curves to the northeast toward Nova Scotia and the Grand Banks.

Six Datawell Directional Waverider buoys (X1 to X6) were deployed along a cross-shelf transect extending almost due east from the Duck beach to the shelf break (Figure 2). The buoys were deployed in water depths of 21m (X1, located 5.35 km from shore); 24 m (X2, 12.78 km); 26 m (X3, 22.17 km from shore); 33 m (X4, 37.74 km from shore); 39 m (X5, 58.22 km from shore); and 193 m (X6, 86.57 km from shore) (Table 1).

Buoy	Distance From Shore	Depth	Latitude	Longitude	Dates Deployed
X1	5.4 km	21 m	36° 13.62' N	75° 42.28' W	9/13/99 – 12/13/99
X2	12.8 km	24 m	36° 13.62' N	75° 36.77' W	9/11/99 – 12/12/99
X3	22.2 km	26 m	36° 12.27' N	75° 29.91' W	9/10/99 – 12/13/99
X4	37.7 km	33 m	36° 09.50' N	75° 19.53' W	9/10/99 – 12/13/99
X5	58.2 km	39 m	36° 07.79' N	75° 06.05' W	9/13/99 – 10/24/99 10/28/99 – 12/13/99
X6	86.62 km	197 m	36° 04.98' N	75° 47.47' W	9/13/99 – 9/21/99
	86.57 km	193 m	36° 04.97' N	75° 47.50' W	10/15/99- 12/5/99

Table 1. Locations and time periods of Datawell Directional Waverider buoys (X1 to X6) deployments

Buoy X5 broke loose on October 24, and was redeployed on October 28. Buoy X6 broke loose on September 21, was redeployed on October 15, and lost again from December 5 through the end of the experiment. All other buoys were operational throughout the experiment.

The Datawell Directional Waverider buoys are surface following directional wave buoys (about 1 m diameter) which measure horizontal and vertical orbital displacements at the sea surface from which wave height spectra and directional wave properties are determined. They contain a heave-pitch-roll sensor (Hippy-40), three axis fluxgate compass, two fixed 'x' and 'y' accelerometers, a temperature sensor and a microprocessor. The direction measurement is based on the translation principle, using the measured horizontal accelerations rather than surface slopes used in earlier pitch-and-

roll type buoys. Therefore, the measurement is independent of buoy roll motions and thus, a small spherical buoy can be used. From the accelerations and tilts measured in the moving 'buoy reference frame,' the accelerations along the fixed horizontal, north and west axes are calculated. All three accelerations (vertical, north and west) are digitally integrated to get filtered displacements with a high frequency cut-off at 0.6 Hz. To save transmitting power, the real time data are compressed to vertical, north and west displacements. Every half hour, Fast Fourier Transforms of 8 series of 256 data points (200 sec) are used to form spectra and cross-spectra with 16 degrees of freedom. Frequency resolutions of 0.005 Hz in the range 0.025 to 0.1 Hz, and 0.01 Hz in the range 0.1 to 0.58 Hz are used. For each frequency bandwidth, the on-board microprocessor computes energy density, mean direction, directional spread, and the normalized second harmonic of the directional distribution (discussed in Chapter III). The Directional Waverider buoy transmits the following information: vertical, north, and west displacements, spectral density, processed directional parameters, sea surface temperature (SST) and other system status with parity bits for error checking purposes. The buoy data, framed in 64 bit vectors, is transmitted via HF in the 27-40 MHz band continuously. The processed spectral and directional data is transmitted 8 times to allow for reliable data return even in marginal transmission conditions.

A single point vertical mooring (Figure 3) ensures sufficient symmetrical horizontal buoy response even for small motions at low frequencies. The Directional Waverider is fitted with 5 kg chain ballast to provide stability when only a vertical mooring force is present (free floating or moored in shallow water). The low stiffness of

the 30 m rubber cord allows the buoy to follow waves up to 40 m in height. High shock accelerations are absorbed by the fluid surrounding the accelerometer and the shockproof mounting of the accelerometer housing, electronics and batteries.

The four buoys located closest to shore (X1 to X4) transmitted their respective data via an HF radio link to receivers mounted on a 50 m high tower at the FRF, while the outer two buoys (X5 and X6) that were out of HF range, used internal data loggers.

Significant weather associated with La Niña conditions played an important role in the formation of long period energetic swell that propagated across the continental shelf during the fall of 1999. Hurricane season peaked in September and October with Hurricanes Floyd, Gert, Irene and José (Figure 4). On September 17, the eye of Hurricane Floyd passed within 100 km of the buoy transect generating large seas on the continental shelf and causing massive flooding and destruction in eastern North Carolina. Hurricanes Gert and José remained offshore but radiated long period swell across the transect of buoys. Hurricane Irene made landfall across western Cuba and southeastern Florida and continued northeastward, following the Gulf Stream and remained offshore of the Carolinas. Further discussion on these storms is found in the case studies in Chapter IV.

III. DATA ANALYSIS

The directional properties of ocean surface waves are often described by the mean wave direction, $\theta_{\text{mean}}(f)$, and the directional spread, $\sigma_{\theta}(f)$, as functions of frequency.

These variables are closely related to the directional distribution of wave energy,

$S(\theta; f)$: $\theta_{\text{mean}}(f)$ is the mean of this distribution, defining a dominant wave propagation direction at each frequency, whereas $\sigma_{\theta}(f)$ represents the standard deviation of the distribution and characterizes the half-width of the directional distribution. Estimates of $\theta_{\text{mean}}(f)$ and $\sigma_{\theta}(f)$ are readily obtained from heave-pitch-and-roll or translational directional wave buoys (e.g., Longuet-Higgins et al., 1963; Mitsuyasu et al., 1975; Long, 1980, Kuik et al., 1988). Longuet-Higgins et al. (1963) showed that the first four directional Fourier coefficients of $S(\theta; f)$ can be derived from the auto-, co- and quadrature spectra of the three basic heave and slope (or horizontal displacement) signals of the buoy. For a Datawell Directional Waverider buoy that measures the horizontal (x,y) and vertical (z) displacements of water particles at the surface, the Fourier moments can be expressed as:

$$a_1(f) \equiv \int_{-\pi}^{\pi} d\theta \cos(\theta) S(\theta; f) = \frac{Q_x(f)}{\{C_z(f)[C_{xx}(f) + C_{yy}(f)]\}^{1/2}} \quad (1)$$

$$b_1(f) \equiv \int_{-\pi}^{\pi} d\theta \sin(\theta) S(\theta; f) = \frac{Q_{zy}(f)}{\{C_{xx}(f)[C_{xx}(f) + C_{yy}(f)]\}^{1/2}} \quad (2)$$

$$a_2(f) \equiv \int_{-\pi}^{\pi} d\theta \cos(2\theta) S(\theta; f) = \frac{C_{xx}(f) - C_{yy}(f)}{C_{xx}(f) + C_{yy}(f)} \quad (3)$$

$$b_2(f) \equiv \int_{-\pi}^{\pi} d\theta \sin(2\theta) S(\theta; f) = \frac{2C_{xy}(f)}{C_{xx}(f) + C_{yy}(f)} \quad (4)$$

where C_{ij} and Q_{ij} denote the co- and quadrature spectra of components i and j respectively.

For narrow $S(\theta)$, θ_{mean} and σ_{θ} can be approximated by the first-order moments,

a_1 and b_1 (e.g., Kuik et al., 1988):

$$\int_{-\pi}^{\pi} d\theta \sin(\theta - \theta_{\text{mean}}) S(\theta) = b_1 \cos(\theta_{\text{mean}}) - a_1 \sin(\theta_{\text{mean}}) = 0 \quad (5)$$

$$\sigma_{\theta}^2 \equiv \int_{-\pi}^{\pi} d\theta (2[1 - \cos(\theta - \theta_{\text{mean}})]) S(\theta) = 2[1 - (a_1 \cos(\theta_{\text{mean}}) + b_1 \sin(\theta_{\text{mean}}))]. \quad (6)$$

For small $\theta - \theta_{\text{mean}}$

$$\sin (\theta - \theta_{\text{mean}}) \approx (\theta - \theta_{\text{mean}}) \left[1 - \frac{1}{6} (\theta - \theta_{\text{mean}})^2 \right]$$

$$2[1 - \cos (\theta - \theta_{\text{mean}})] \approx (\theta - \theta_{\text{mean}})^2 \left[1 - \frac{1}{12} (\theta - \theta_{\text{mean}})^2 \right]$$

and thus, θ_{mean} and σ_θ represent a mean value and standard deviation of the directional distribution of wave energy with an $O(\theta - \theta_{\text{mean}})^2$ bias.

A disadvantage of this formulation is the sensitivity of σ_θ to directionally opposing wave components. A small amount of wave energy traveling in a direction opposing the dominant swell system (e.g., reflection of waves from shore or a weak secondary swell peak) causes a large increase in the σ_θ estimate that is not related to the beam width of the dominant swell (Herbers et al, 1999).

Alternatively, θ_{mean} and σ_θ can be defined in terms of the second-order moments a_2 and b_2 (e.g., Herbers et al., 1999):

$$\int_{-\pi}^{\pi} d\theta \frac{1}{2} \sin [2(\theta - \theta_{\text{mean}})] S(\theta) = \frac{1}{2} [b_2 \cos (2\theta_{\text{mean}}) - a_2 \sin (2\theta_{\text{mean}})] = 0 \quad (7)$$

$$\sigma_\theta^2 \equiv \int_{-\pi}^{\pi} d\theta \frac{1}{2} \{ [1 - \cos [2(\theta - \theta_{\text{mean}})]] \} S(\theta) = \frac{1}{2} [1 - (a_2 \cos (2\theta_{\text{mean}}) + b_2 \sin (2\theta_{\text{mean}}))] \quad (8)$$

For small $\theta - \theta_{\text{mean}}$

$$\frac{1}{2} \sin [2(\theta - \theta_{\text{mean}})] \approx (\theta - \theta_{\text{mean}}) [1 - \frac{2}{3} (\theta - \theta_{\text{mean}})^2]$$

$$\frac{1}{2} \{1 - \cos[2(\theta - \theta_{\text{mean}})]\} \approx (\theta - \theta_{\text{mean}})^2 [1 - \frac{1}{3} (\theta - \theta_{\text{mean}})^2]$$

and therefore the second-order approximations of θ_{mean} and σ_θ have larger biases than the first-order approximations, Eqs 5 and 6. However, Eqs 7 and 8 are much less sensitive than Eqs 5 and 6, to a weak directionally opposing wave system, because the double-angle argument, $2(\theta - \theta_{\text{mean}})$, is the same for waves propagating in opposite directions. Unlike the first-order estimate of θ_{mean} (Eq 5), the second-order estimate has a 180° ambiguity.

In the present analysis, estimates of θ_{mean} and σ_θ were obtained from both the first- and second-order moments. Because the two methods have different errors, intercomparison of θ_{mean} and σ_θ estimates based on a_1 , b_1 and a_2 , b_2 (discussed below) provides a useful check of the accuracy of the estimates. A magnetic correction of -10.75° W was applied to $\theta_{\text{mean}}(f)$, and the resulting direction was transformed to nautical convention, that is the transformed $\theta_{\text{mean}}(f)$ is the direction the waves come from, measured counterclockwise from true north. In addition to θ_{mean} and σ_θ estimates as functions of frequency, bulk estimates were computed for the frequency range 0.025 to

0.25 Hz. The estimates are based on Eqs 5-8 using energy-weighted average values of the moments, a_1 , b_1 and a_2 , b_2 :

$$a_{1_{total}} = \frac{\int_{0.025 \text{ Hz}}^{0.25 \text{ Hz}} a_1(f) E(f) df}{\int_{0.025 \text{ Hz}}^{0.25 \text{ Hz}} E(f) df} \quad (9)$$

$$b_{1_{total}} = \frac{\int_{0.025 \text{ Hz}}^{0.25 \text{ Hz}} b_1(f) E(f) df}{\int_{0.025 \text{ Hz}}^{0.25 \text{ Hz}} E(f) df} \quad (10)$$

$$a_{2_{total}} = \frac{\int_{0.025 \text{ Hz}}^{0.25 \text{ Hz}} a_2(f) E(f) df}{\int_{0.025 \text{ Hz}}^{0.25 \text{ Hz}} E(f) df} \quad (11)$$

$$b_{2_{total}} = \frac{\int_{0.025 \text{ Hz}}^{0.25 \text{ Hz}} b_2(f) E(f) df}{\int_{0.025 \text{ Hz}}^{0.25 \text{ Hz}} E(f) df} \quad (12)$$

where $E(f)$ [$\equiv C_z(f)$] is the wave frequency spectrum.

A preliminary analysis of the bulk wave and wind parameters during the entire experiment was conducted to select specific events for further analysis. For each case

covering time periods of 12 or 3 hours, the spectra of the half-hour data records were ensemble averaged, and directional moments, $\theta_{\text{mean}}(f)$ and $\sigma_{\theta}(f)$, were computed based on the ensemble averages of the moments (a_1 , b_1 , a_2 , and b_2) weighted by $E(f)$. The resulting $E(f)$, $\theta_{\text{mean}}(f)$, and $\sigma_{\theta}(f)$ have approximately 384 degrees of freedom.

IV. CASE STUDIES

The times of the selected twelve case studies are listed in Table 2, together with the significant wave height:

$$H_s = 4 \sqrt{\int_{0.025 \text{ Hz}}^{0.25 \text{ Hz}} E(f) df}, \quad (13)$$

the peak period, T_p , (the wave period corresponding to the peak of the spectrum, $E(f)$), and the bulk θ_{mean} and σ_θ parameters (calculated using Eqs 5-12) all from the offshore buoy, and the wave height decay across the shelf quantified by the ratio $H_s(X1)/H_s(X6)$.

Eight of the cases were collected during light wind conditions on the shelf when the wave field was dominated by remotely generated long period ($T_p=12-17$ s) swell. Since it takes several hours for the swell to traverse the shelf, 12-hour periods were used in the analysis with relatively steady significant wave heights, peak periods and mean propagation directions.

Six of the swell cases are "easterly swell" events with mean offshore directions within $\pm 45^\circ$ of 090° T. The easterly swell cases include forerunners from Hurricane Floyd and arrivals from Hurricane Gert. Hurricane Gert was a category IV hurricane that was tracking to the northwest and slowly turned north-northeastward on September 21. Gert's closest point of approach was about 1100 km to the southeast of the buoy transect

(Figure 4). Gert produced the longest period ($T_p = 15\text{-}17$ s) and directionally narrowest ($\sigma_\theta = 20\text{-}24^\circ$) swells of the experiment.

EASTERLY SWELL	H_s at X6	T_p at X6	θ_{mean} at X6	σ_θ at X6	$\frac{H_s(X1)}{H_s(X6)}$
09/14 00 EST to 09/14 12 EST (FLOYD)	2.90 m	13.33 s	134.7° T	29.6°	0.57
09/19 12 EST to 09/20 00 EST (GERT)	2.78 m	15.38 s	124.3° T	20.4°	0.47
09/20 21 EST to 09/21 09 EST (GERT)	2.54 m	16.67 s	127.0° T	24.4°	0.55
09/23 16 EST to 09/24 04 EST	X5: 1.47 m	X5: 12.50 s	X5: 73.4° T	X5: 42.5°	(X1)/(X5): 0.63
11/18 03 EST to 11/18 15 EST	1.19 m	14.29 s	54.5° T	36.5°	0.66
11/22 18 EST to 11/23 06 EST	2.07 m	11.76 s	97.0° T	34.8°	0.67
LARGE OBLIQUE ANGLE SWELL					
10/23 02 EST to 10/23 14 EST (JOSE)	1.70 m	12.50 s	163.4° T	50.6°	0.51
12/01 21 EST to 12/02 09 EST	4.60 m	13.33 s	034.8° T	31.2°	0.50
STORM WAVES					
09/16 09 EST to 09/16 12 EST (FLOYD)	7.63 m	12.50 s	180.0° T	27.1°	0.62
10/18 00 EST to 10/18 03 EST (IRENE)	4.30 m	10.00 s	161.3° T	30.0°	0.62
11/02 20 EST to 11/02 23 EST	5.00 m	10.00 s	167.9° T	31°	0.42
11/11 23 EST to 11/12 02 EST	3.58 m	9.09 s	020.3° T	28.2°	0.77

Table 2. Twelve case studies classified as: “Easterly Swell”, “Large Oblique Angle Swell” and “Storm Waves” listed at the offshore buoy, X6, are: Significant wave height, H_s ; peak period, T_p ; bulk mean propagation direction, θ_{mean} ; and bulk directional spread, σ_θ . Also listed is the wave height decay between X1 and X6.

In the remaining two cases, swell arrived at very large angles to shore-normal resulting in strong refraction effects. The two “large oblique angle swell” cases include southerly swell from Hurricane José and a northerly swell case. Hurricane José remained well offshore and followed a somewhat similar track to Hurricane Gert, traveling to the north-northwest until passing the eastern tip of Puerto Rico before recurving to the north-

northeast (Figure 4). José's closest point of approach was 900 km of the buoy transect to the southeast. The southeasterly swell from José propagated over the steep slope of the continental shelf located to the southeast of the buoy transect (Figure 1) near Cape Hatteras Point. In contrast, waves arriving from northerly directions travel a long distance over the continental shelf, which widens and curves to the northeast.

In addition to the 8 swell cases, 4 storm cases with strong winds and active wave generation on the continental shelf, were selected for analysis. Because of the more rapidly varying conditions, 3-hour periods at the peak of the storm events were analyzed. These cases include Hurricanes Floyd and Irene, the most significant storm events during the entire 3-month experiment. Their tracks passed within 100-200 km from the buoy transect and produced large waves (maximum H_s of 4.3 – 7.6 m) on the continental shelf. Figure 5 displays the associated winds and H_s of Hurricanes Floyd and Irene. The peak winds of 35 m/s for Floyd occurred around 2000 EST on September 16 (well after Hurricane Floyd made land fall) while the peak H_s at buoy X6 were observed about 2 hours later (Figure 5a). Since Floyd passed to the west of the buoy transect (Figure 4), the strongest winds were observed closest to shore as indicated by the difference in maximum wind speeds between FRF and NOAA Buoy 44014 observations. The NOAA Buoy 44014 was located about 30 km northeast of the buoy transect (Figure 1). Hurricane Irene made landfall over southeastern Florida, but remained offshore of the Carolinas, and passed within 250 km of the buoy transect (Figure 4). As Irene passed to the southeast of the transect, the dominant waves continued to arrive from the south-

southeast even though the strong local winds (on the west side of the hurricane) were from the northwest (Figure 5b).

The other two storm events selected were local storms (a cold frontal system on November 2 and a nor'easter on November 11-12) that produced comparably large waves on the shelf. In the Floyd, Irene and the November 2 storm events, when the dominant seas observed at X6 arrived from the south, strong refraction and fetch-limited conditions on the inner shelf were expected. The nor'easter case shows very different conditions of fetch-unlimited seas generated by northeasterly winds.

The November 2 storm moved slowly across the study site with wind speed observations from the FRF at a maximum of 18 m/s at 1200 EST while the NOAA buoy's peak wind speed occurred about 10 hours later, during the 3-hour period selected (Figure 6a). In contrast, the nor'easter storm quickly passed through the study area with the peak wind observations at the NOAA buoy occurring 3-4 hours later than at the FRF. H_s was at a maximum at buoy X6 about 2 hours after the peak wind observations from the FRF station (Figure 6b).

For each case the transfer function, $G(f)$, was examined between the horizontal and vertical displacements, to verify the buoy response:

$$G(f) = \sqrt{\frac{C_{xx}(f) + C_{yy}(f)}{C_{zz}(f)}} \quad (14)$$

For linear waves $G(f) = 1 / \tanh(k(f) h)$, where h is the water depth and the wavenumber, k , is given by the dispersion relation $(2\pi f)^2 = gk \tanh(kh)$. Hence, the

normalized transfer function $G'(f) [= \tanh(k(f)h) G(f)]$ is equal to 1 for linear waves. Nonlinearities in both the wave field and buoy response will result in deviations of G' from 1. Bulk values of G and G' integrated over the spectra are expressed as:

$$G = \sqrt{\frac{\int_{0.025 \text{ Hz}}^{0.25 \text{ Hz}} C_{xx}(f) + C_{yy}(f) df}{\int_{0.025 \text{ Hz}}^{0.25 \text{ Hz}} C_{zz}(f) df}} \quad (15)$$

$$G' = \sqrt{\frac{\int_{0.025 \text{ Hz}}^{0.25 \text{ Hz}} \tanh(k(f)h) [C_{xx}(f) + C_{yy}(f)] df}{\int_{0.025 \text{ Hz}}^{0.25 \text{ Hz}} C_{zz}(f) df}} \quad (16)$$

Figure 7a shows the observed ratio, G , for each of the twelve cases. The observed ratios are close to 1 at the deep water (buoy X6), but, for all cases, G generally increases from the outer shelf to the inner shelf. This trend is consistent with the transformation of the wave orbital motion from deep (circular orbits, $G = 1$) to shallow (ellipsoidal orbits, $G > 1$) water. The normalized ratios vary between 1 to 1.2 (Figure 7b), showing a slight but systematic positive bias that increases with distance from shore, possibly due to nonlinear effects.

The accuracy of the directional moments, θ_{mean} and σ_{θ} , is verified in Figure 8 by comparing the estimates based on the second-order approximations (a_2 , b_2) for each of

the twelve cases listed in Table 2, with their respective estimates based on first-order approximations (a_1, b_1) . The bulk θ_{mean} values obtained with the two different approximations are in excellent agreement (Figure 8a). However, the σ_θ values are well correlated but estimates based on (a_2, b_2) values are generally about 15-25% smaller than estimates based on (a_1, b_1) (Figure 8b). These differences are qualitatively consistent with the larger negative bias expected for σ_θ estimates based on the second-order moments discussed earlier. The estimates of θ_{mean} and σ_θ used in Chapters V and VI for the preliminary analysis of the twelve cases are based on the less-biased first-order approximations (a_1, b_1) .

V. CROSS-SHELF VARIATIONS

Variations in wave properties across the continental shelf can result from different attenuation mechanisms discussed in Chapter 1. Bottom friction, refraction of waves arriving at oblique angles, and fetch limitations of wave growth on the continental shelf all contribute to a decrease in wave height across the shelf, causing sheltered conditions near the coast. In this Chapter, a preliminary analysis of the observed variations in H_s , θ_{mean} , and σ_θ across the shelf is presented.

A. EASTERLY SWELLS

The cross-shelf variations for the six easterly swell cases (Table 2) are displayed in Figures 9 and 10. In all six cases, a large decrease in wave heights across the shelf is observed, with H_s at buoy X1 on the inner shelf that are between 33 and 53% smaller than H_s values measured with buoy X6 on the outer shelf. These decreases in wave height are much larger than the variations resulting from shoaling and refraction (Herbers et al., 2000), suggesting that the strong attenuation of swell is caused by bottom friction. The strongest decay is observed for the most energetic swells generated by Hurricanes Floyd (September 14) and Gert (September 19 and 20). Although the overall decay is comparable for these two events, the cross-shelf evolution is different. During Hurricane Floyd, strong initial swell decay (~37% decrease in H_s) is observed across the outer shelf between buoys X6 and X5, followed by weaker variations across the mid- and inner shelf. During Hurricane Gert, a dramatic decrease in H_s (between 25 and 37%) is observed on the inner shelf between buoys X3 and X2, with weaker variations offshore of

buoy X3 and inshore of buoy X2. The remaining three cases show a more gradual wave decay across the shelf.

The easterly swell cases are characterized by bulk θ_{mean} ranging from 050° to 135° T (Figure 10a). The coastline and continental shelf break are oriented at $\sim 070^\circ$ T and 100° T, respectively, and thus, the observed θ_{mean} correspond to small ($< 45^\circ$) angles of incidence. Variations of θ_{mean} across the shelf are small, except for the more southerly Floyd and Gert cases that show a $\sim 30^\circ$ shift toward normal incidence. In most cases, the bulk σ_θ remained either fairly steady (between 35° and 28°) or show a slight narrowing across the shelf that is likely due to weak refraction effects. The cases associated with Hurricane Gert with narrow offshore spectra ($\sigma_\theta \approx 20^\circ$) show a sharp increase of σ_θ of 30% across the inner shelf (buoy X3 to X1) (Figure 10b), possibly due to wave scattering from bottom irregularities.

B. LARGE OBLIQUE ANGLE SWELLS

In the two oblique angle swell cases shown in Figure 11, swells approach the shelf break at near grazing ($\approx 65^\circ$ relative to normal incidence) northeasterly (December 11) and southeasterly (October 23) angles. In both cases the significant wave height, H_s , decreased by about 50% across the shelf (i.e., energy reduction of a factor of 4) (Figure 11a). This decay is likely caused by a combination of refraction and bottom friction.

In both oblique angle cases, refraction effects are evident in the gradual turning of θ_{mean} across the continental shelf toward smaller oblique angles (Figure 11b). However, the observed refraction of the southeasterly swell from Hurricane José is much stronger

(from 165° T at buoy X6 to 105° T at X1) than in the northeasterly swell case where the change is less significant with swells arriving (from 035° T at buoy X6 to 055° T at X1). These direction shifts are qualitatively consistent with refraction computations presented in Herbers et al. (2000, cf. their Figure 3d).

The σ_θ (Figure 11c) observed in the northeasterly case is fairly uniform across the shelf (about 30° to 40°). In contrast, the southeasterly swells are broader at the offshore buoys, X5 and X6 ($\sigma_\theta \approx 50$ -55°) narrowing to 38° at the inner shelf buoy X1. The unusually large σ_θ offshore does not appear to be related to the shelf topography (buoy X6 is in deep water) and suggest possible scattering effects of the Gulf Stream.

C. STORM WAVES

The cross-shelf evolution of seas generated by Hurricanes Floyd, Irene and the local November 2 storm are presented together in Figure 12. The dominant waves arrived from south-southeast directions in all three cases, indicating fetch-limited conditions on the shelf. The nor'easter storm is an unlimited fetch case with waves arriving from unobstructed north-northeast directions. Therefore, the nor'easter case is presented separately in Figure 13.

In the three fetch-limited cases, the observed wave heights decrease across the continental shelf by about 40-50% between buoys X6 and X1 (Figure 12a). These H_s reductions on the inner shelf are comparable to the decay observed in swell conditions (cf. Figures 10, 12a), but the mechanisms may be quite different as waves are actively generated on the shelf. In all three cases, the θ_{mean} estimates show waves arriving from south-southeasterly directions at the outer shelf buoys, X6 and X5, shifting by about 60-

65° to near shore-normal directions at buoy X1 (115-120° T). The large differences observed between the dominant wave and wind directions on the inner shelf (e.g., southerly winds and easterly waves during Floyd) can be explained by the extremely limited fetch for southerly winds and the strong refraction of waves propagating nearly parallel to the local depth contours (Figure 12b). In all three cases $\sigma_\theta \approx 25\text{-}30^\circ$ at the outer shelf buoys (X4-X6), but the estimates diverge on the inner shelf (Figure 12c). In Hurricane Irene σ_θ increases to 45° at buoy X1, whereas the σ_θ values of Hurricane Floyd and the local November storm case decrease slightly to 20-25° at buoy X1. These differences are discussed in Chapter VI. Variations of H_s , θ_{mean} , and σ_θ observed in the nor'easter case are small (Figure 13). H_s decreased by only 25% across the continental shelf. The observed θ_{mean} are about 020°-025° T at buoys X6 and X5, shifting to 040°-045° T at buoys X4 to X1. The σ_θ are nearly uniform across the buoy transect varying from 25°-30°. These weak variations indicate that refraction is of lesser importance in a nor'easter, and that the wave field is fully developed in equilibrium with the wind.

VI. FREQUENCY DIRECTIONAL SPECTRA

The evolution of the frequency-directional wave spectrum, $S(\theta; f)$, across the continental shelf is examined in detail for the four storm wave events: Hurricanes Floyd, Irene, the November 2 storm, and the nor'easter.

Estimates of $E(f)$, $\theta_{\text{mean}}(f)$, and $\sigma_{\theta}(f)$ at the peak of Hurricane Floyd are shown in Figure 14. The frequency spectra, $E(f)$, (Figure 14a) show a large decrease in spectral levels between offshore buoy X6 and inner shelf buoy X1 in the frequency range 0.08 to 0.12 Hz that corresponds to the peak of the offshore spectrum. The spectral peak level decreases monotonically from the outer shelf to the inner shelf (about a factor of 5 between buoys X6 and X1), even though the maximum winds of 35 m/s were observed at the FRF station close to the inner shelf buoys (Figure 5a). At both higher frequencies and lower frequencies, the spectrum is nearly uniform across the shelf. The decrease in wind sea peak energy on the inner shelf may be caused by bottom damping and/or limited fetch.

The $\theta_{\text{mean}}(f)$ estimates show large cross-shelf variations caused by refraction (Figure 14b). At the outer shelf buoys, X5 and X6, southerly angles (180° T through 200° T) are observed at all frequencies. Between buoys X5 and X1, a shift in direction is observed that is largest for the lower frequencies. This is qualitatively consistent with refraction that is strongest for low frequency waves that feel the bottom over the entire shelf. For example, at buoy X1, the mean direction at high frequencies is about 190° T (close to the local wind direction), and decreases with decreasing frequency to 120° T

(near normal incidence) at the spectral peak. Topographic effects play an important role in the evolution of lower frequency waves, but have little effect on the high frequency waves that are in equilibrium (i.e., saturated) with the local wind.

For all six buoys, $\sigma_\theta(f)$ is narrowest at the spectral peak (15°-25°), and broadens at both higher and lower frequencies (Figure 14c). No systematic variations of $\sigma_\theta(f)$ across the shelf are observed, but at most frequencies, the spreads are generally narrowest at the inner shelf buoys (X1-X3) and widest at the outer shelf buoys (X4-X6).

Although Hurricane Irene passed to the southeast of the buoy transect, producing different conditions on the shelf compared to Hurricane Floyd, there are many similarities in the spectra. The spectral levels were not as high as during Floyd, but the variations of spectral levels across the shelf are similar with about a factor of 5 reduction between X6 and X1 at the spectral peak and weak variations at lower and higher frequencies.

At low frequencies, the $\theta_{\text{mean}}(f)$ estimates of Irene are similar to those observed during Floyd, showing angles of refraction from about 180° to 120° at inner shelf buoy X1 (Figure 15b). At high frequencies (> 0.15 Hz) a wide range of directions is observed. At X1, high-frequency waves arrive from the northeast while at X6, south-southeasterly angles are observed (Figure 15b). These differences can be explained based on the local wind observations. At the time of the analysis, Irene was just passing to the south of the buoy transect and the winds were rapidly shifting from south to north at the FRF station, while wind measured at the NOAA buoy remained in the southerly direction until much later in the day on October 18 (Figure 5b). The high frequency part of the spectrum

apparently responds rapidly to the sudden shift in wind direction on the inner shelf, resulting in a shift to northeasterly directions at buoys X1 and X2.

The corresponding $\sigma_\theta(f)$ estimates show a large increase in spreading at high frequencies between the outer shelf (30-45°) and the inner shelf (55-70°) that is likely caused by bimodal directional spectra on the inner shelf with new northeasterly seas and old southeasterly swells. At lower frequencies, the $\sigma_\theta(f)$ estimates are similar to those observed in Floyd with smaller values at the spectral peak frequency and weak variations across the shelf.

In the November 2 storm case, the energy spectrum decreases uniformly across the shelf (Figure 16a). At all frequencies, spectral levels at buoy X1 are almost an order of magnitude smaller than those observed at X6. This large decrease is consistent with large variations of winds across the shelf. The outer shelf experienced much stronger southerly winds (19 m/s at the NOAA Buoy) than the inner shelf (9 m/s at the FRF) (Figure 6a). Estimates of $\theta_{\text{mean}}(f)$ (Figure 16b) show a large shift from southwesterly directions on the outer shelf to southeasterly directions on the inner shelf. At buoy X6, high frequency components propagate in roughly the local southerly wind direction. But at buoy X1, the local wind (200° T, Figure 6a) and high frequency wave directions (135° T, Figure 16b) differ by 75°. These observations indicate that high frequency waves observed on the inner shelf are generated by stronger winds on the outer shelf and refracted over the sloping shelf bathymetry. At high frequencies, the $\sigma_\theta(f)$ estimates show a systematic decrease across the shelf (Figure 16 c) with much narrower spread at buoy X1 (25°-30°), compared with buoy X6 (45°-50°), that is qualitatively consistent

with the expected directional narrowing of waves refracting from grazing angles toward normal incidence.

The nor'easter case on November 11 shows weaker variation across the shelf compared to the previous cases. At high frequencies, spectral levels are uniform across the shelf, characteristic of a saturated spectral tail in equilibrium with the wind. At low frequencies (< 0.15 Hz) spectral levels decrease monotonically across the shelf, suggesting attenuation of long waves by bottom friction (Figure 17a). At the peak frequency (0.11 Hz), the spectral decay between buoys X6 and X1 is about a factor of 2. At all buoys, $\theta_{\text{mean}}(f)$ is within the range 15° - 45° , close to the wind direction, except at very low frequencies (cf. Figures 17b and 6b). The $\sigma_\theta(f)$ estimate is very similar at all six buoys, with smallest values of 20 - 25° at the spectral peak, broadening at lower and higher frequencies (Figure 17c).

The directional spread observed for all twelve cases is summarized in Figure 18. The common trend for all buoys is a minimum spread at the spectral peak ($f/f_p = 1$), and increasing spread for both lower ($f/f_p < 1$) and higher ($f/f_p > 1$) frequencies. These observations are consistent with deep water observations by Mitsuyasu et al. (1975) and Hasselmann et al. (1980). The range of spread values at $f=f_p$ (listed in Table 3) does not vary much between the outer and inner shelf buoys. At higher frequencies the observed directional spreads are more variable on the inner shelf (cf. buoys X1 and X6), reflecting the complex wind generation (i.e., limited fetch) and topographic effects (e.g., strong refraction along coast hugging waves, scattering effects) near the coast that can both increase or decrease the directional spread.

Buoy	Directional Spread Range at f_p
X1	13° to 34°
X2	14° to 28°
X3	12° to 29°
X4	10° to 28°
X5	12° to 27°
X6	12° to 29°

Table 3. Directional spread range for buoys X1 to X6 at $f/f_p=1$ in Figure 18.

THIS PAGE INTENTIONALLY LEFT BLANK

IV. CONCLUSIONS

During the SHOWEX (SHOaling Waves EXperiment), a cross-shelf transect of six Datawell Directional Waverider buoys was deployed on the North Carolina continental shelf to investigate the transformation of wind-sea and swell spectra in shallow water. A wide range of wave conditions was observed during the three month deployment including several major hurricanes. A preliminary analysis of the buoy observations is presented here. Estimates of the significant wave height, H_s , frequency spectrum, $E(f)$, mean direction, $\theta_{\text{mean}}(f)$, and directional spread, $\sigma_\theta(f)$ were extracted from the buoy measurements using standard techniques. The evolution of wave properties across the shelf is examined to evaluate the relative importance of bottom friction, refraction effects, and limited wind fetch.

The analysis is focused on twelve case studies that include remotely generated swell from Hurricanes Floyd, Gert and José, energetic wind sea conditions during the passage of Floyd and Irene, and a typical nor'easter for this region. In all swell cases, a large (33-53 %) decrease in wave height across the shelf was observed that confirms the dominant role of bottom friction in the transformation of swell across a wide continental shelf. These results are consistent with earlier observations at the same site (Herbers et al., 2000).

Estimates of $\theta_{\text{mean}}(f)$ show the gradual refraction of waves toward shore-normal directions. For swells arriving at the shelf break at a large oblique southerly angle, θ_{mean}

shifts of up to 90° are observed on the inner shelf, enhancing the wave height decay across the shelf.

During the passage of Hurricane Floyd, wave heights decreased from 7.8 m at the shelf break to 4.9 m on the inner shelf even though the strongest winds were observed near the coast. Possible mechanisms that contribute to the wave height decrease are enhanced bottom friction in shallow water, limited fetch on the inner shelf for southerly winds and strong refraction. Similar evolution was observed during Hurricane Irene. In contrast, weak wave heights decay (23% decay) between the offshore and inner shelf buoys) was observed during a nor'easter storm. Waves are more uniform in this case because the fetch is unlimited for northeasterly winds and refraction effects are weaker for waves arriving from northeasterly directions.

For all twelve cases at all six buoys, the $\sigma_\theta(f)$ estimates consistently show a minimum (25° to 30°) near the spectral peak frequency. Cross-shelf variations of σ_θ are generally small, with the exception of the directionally narrowest, Hurricane Gert swell observations that show a dramatic broadening across the inner shelf possibly owing to bottom scattering effects.

APPENDIX. FIGURES

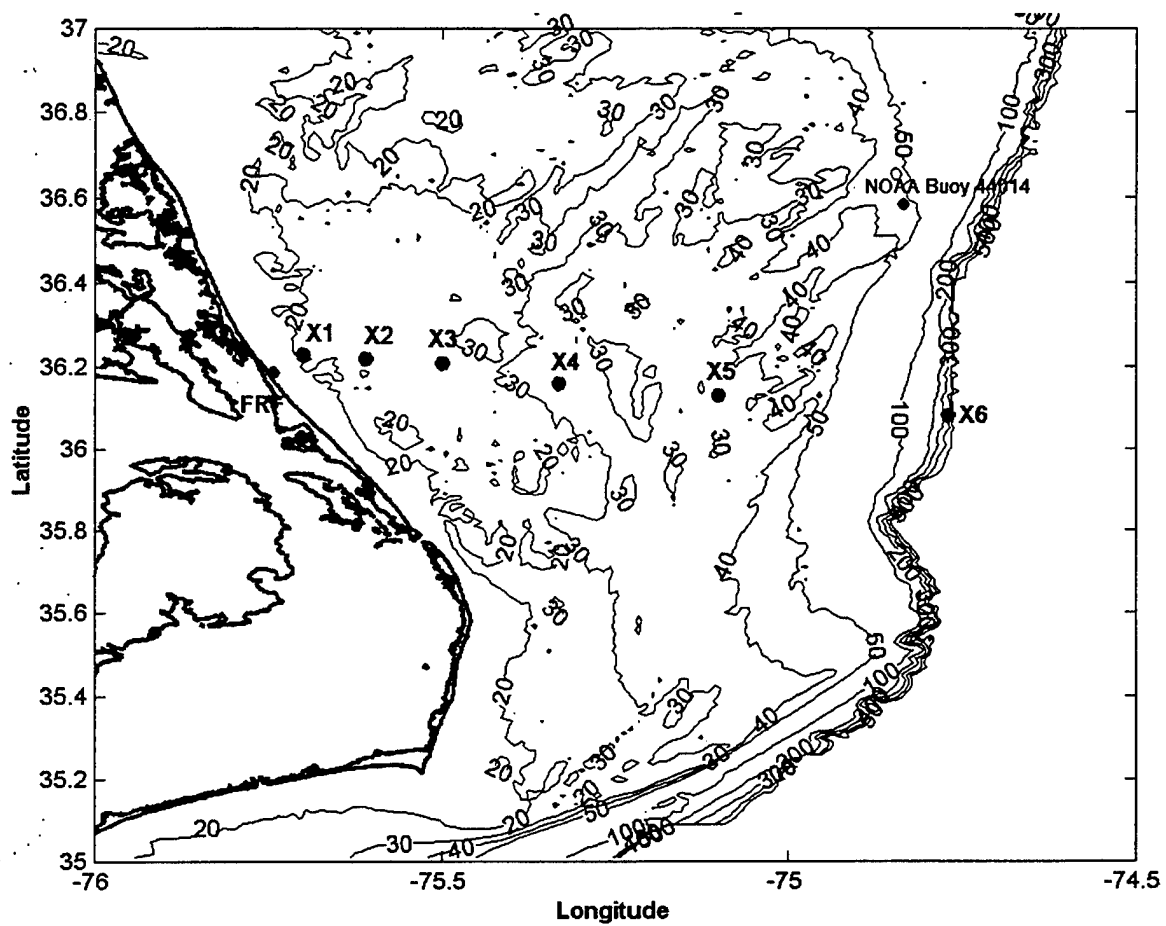


Figure 1. Locations of Datawell Directional Waverider buoys X1 to X6 across the continental shelf.

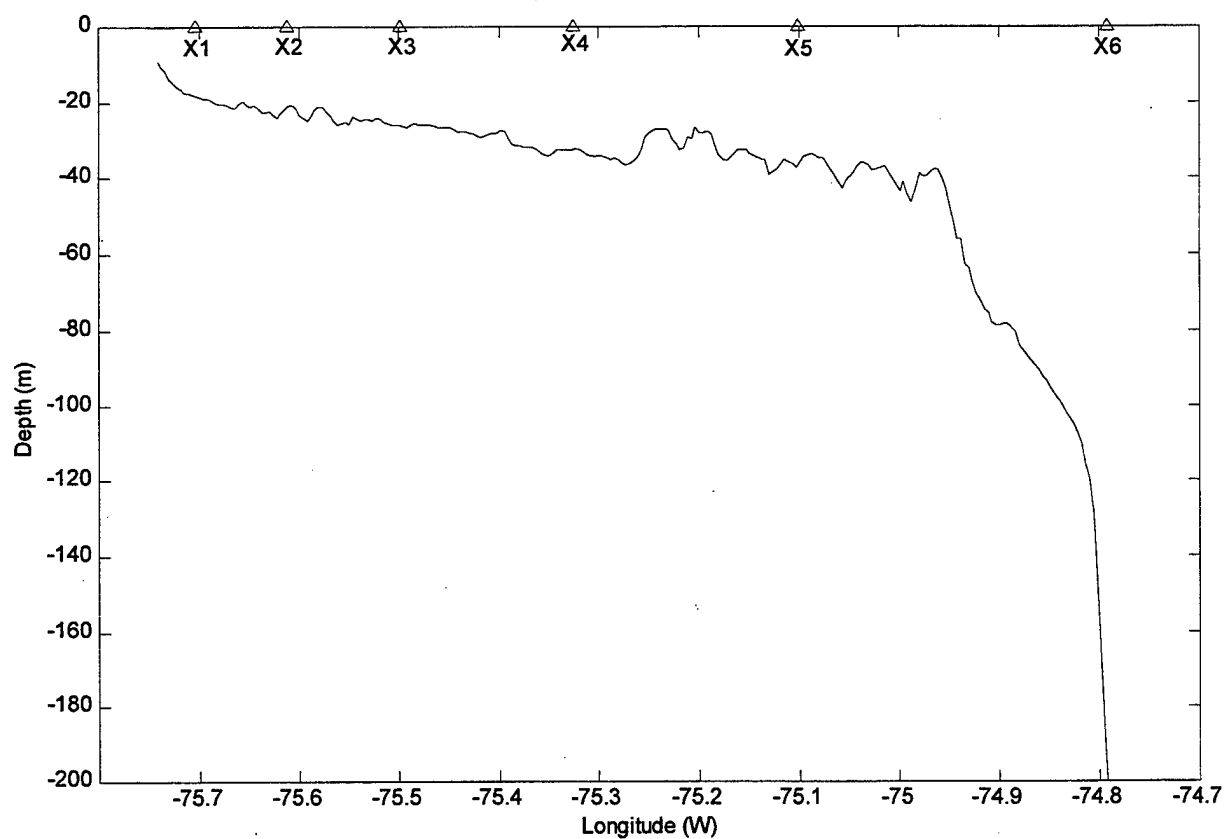


Figure 2. Bottom profile along the cross-shelf transect. The locations of the Datawell Directional Waverider buoys (X1 to X6) are indicated with triangles.

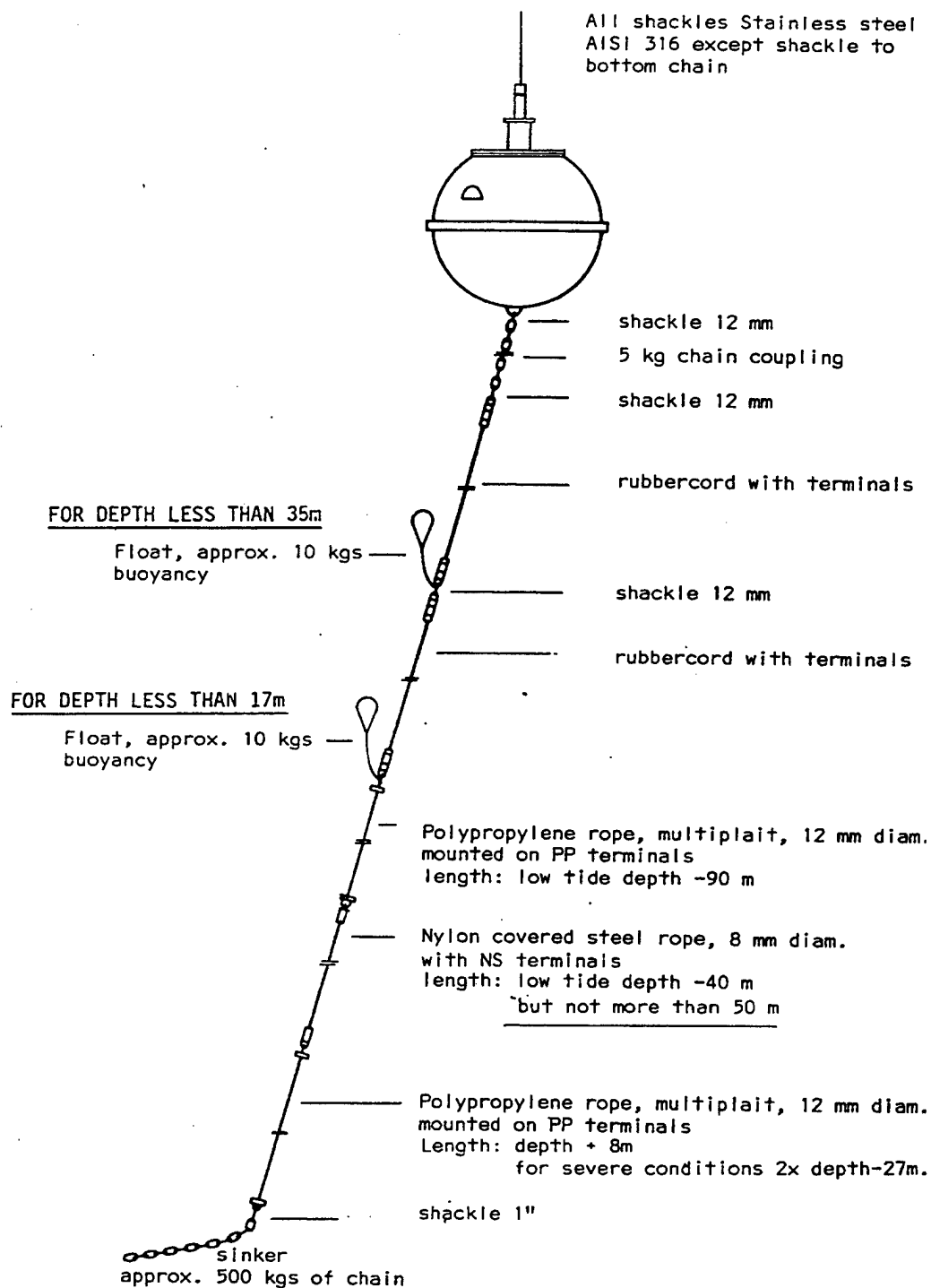


Figure 3. Diagram of a Datawell Directional Waverider buoy and mooring (Datawell by, 1995).

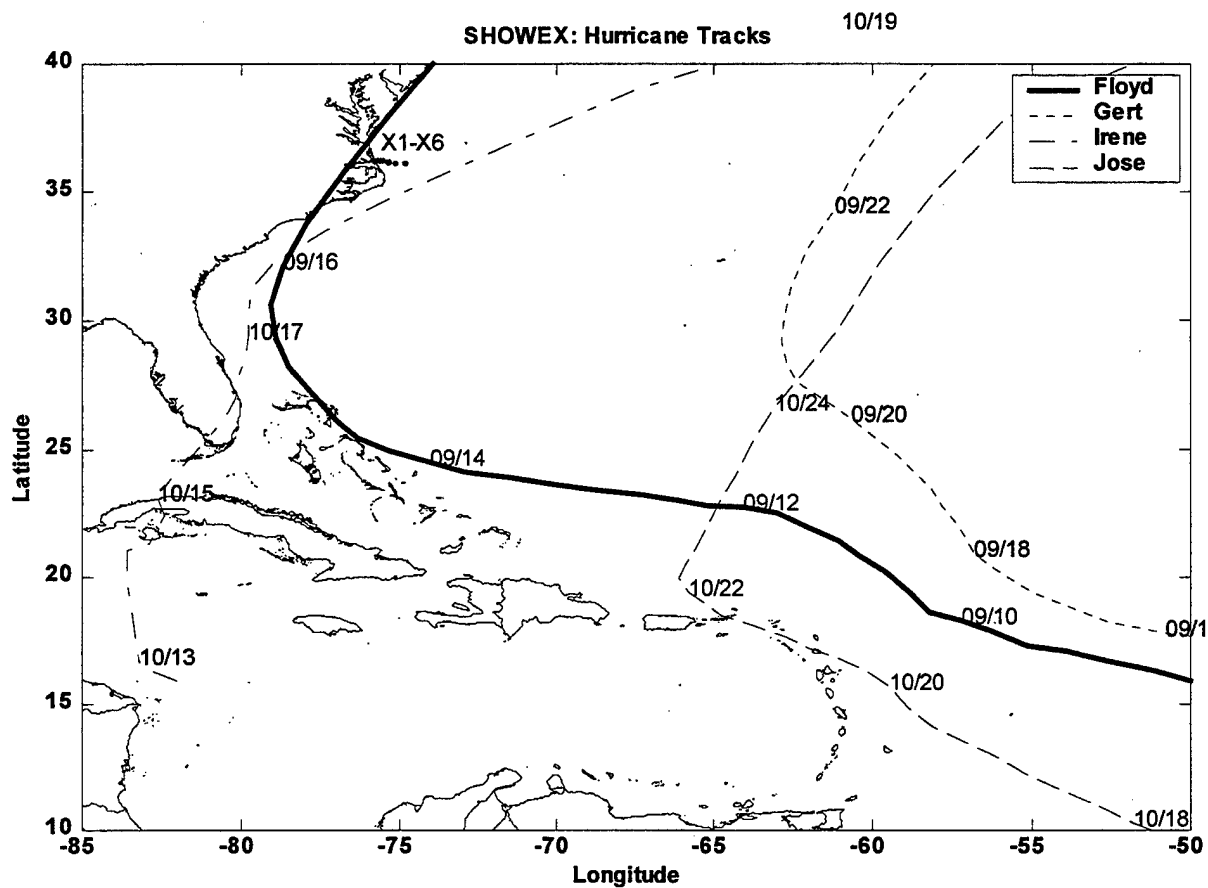


Figure 4. Hurricane tracks for Floyd, Gert, Irene and José in 1999.

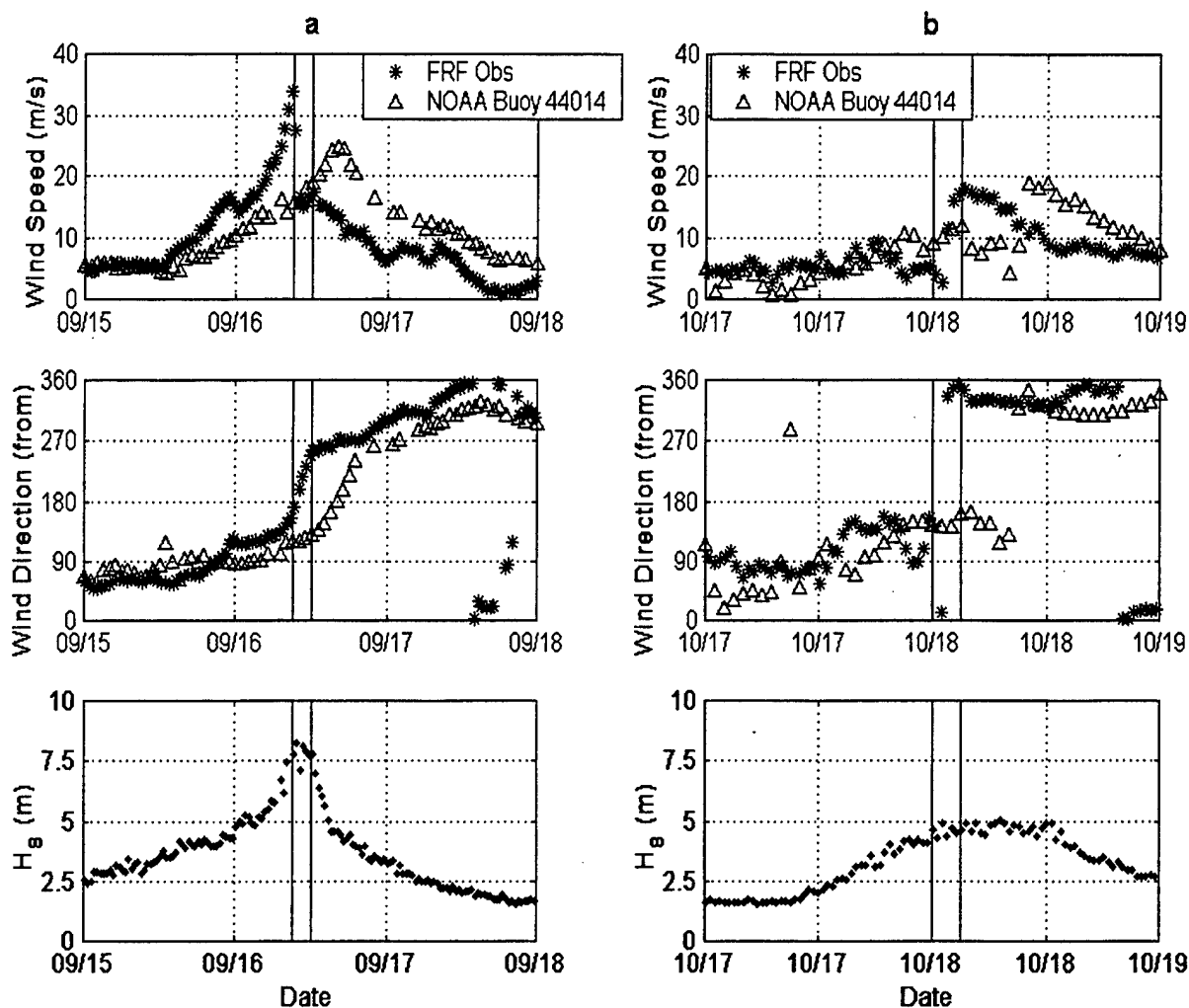


Figure 5. Time series of wind and wave observations during a) Hurricane Floyd: September 15-18, 1999, and b) Hurricane Irene: October 17-19, 1999. Wind speed observations from the FRF station and NOAA buoy 44014 (top), wind direction (middle) and significant wave height, H_s at the offshore buoy, X6 (bottom). The vertical lines indicate the time period analyzed for each event.

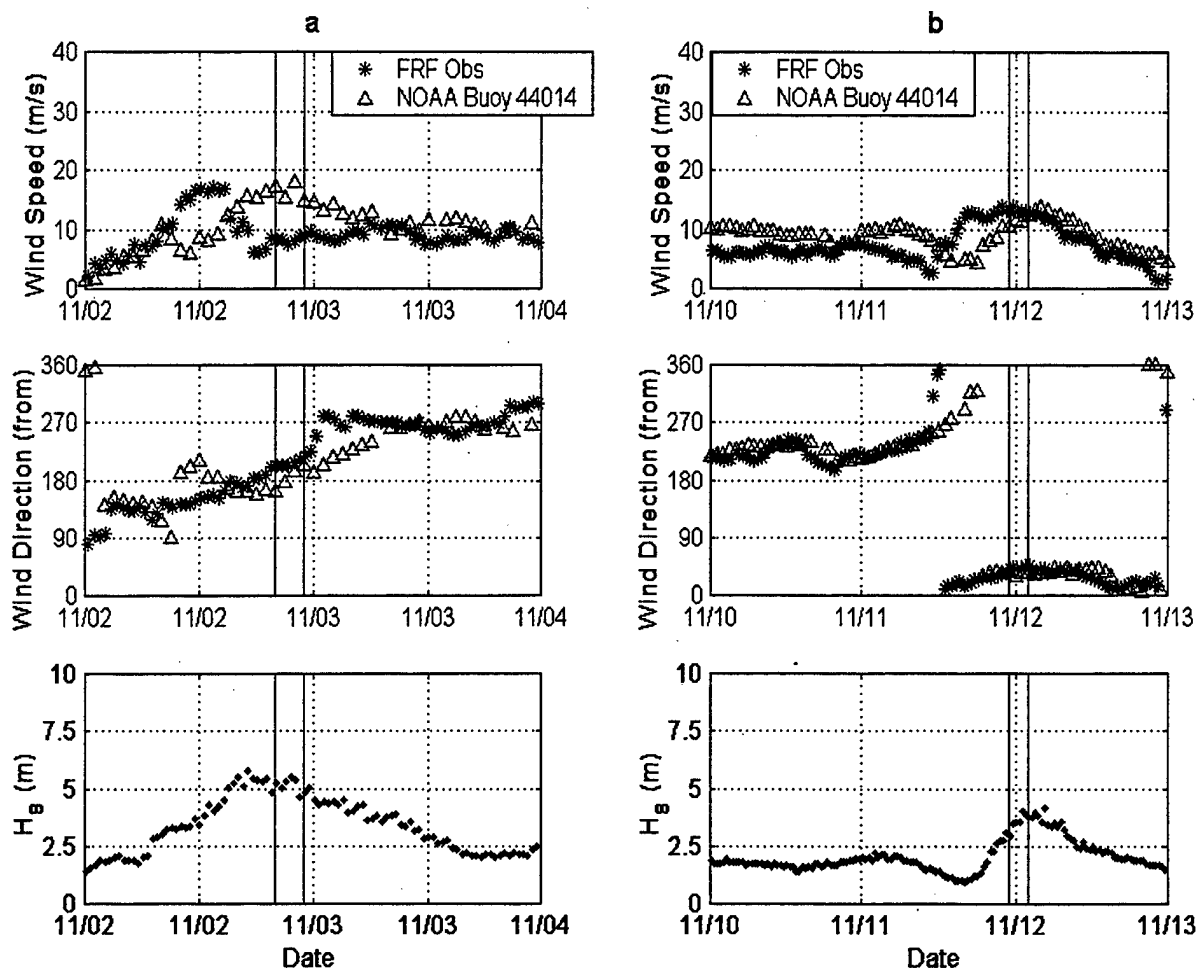


Figure 6. Time series of wind and wave observations during a) a storm on November 2-4, 1999, and b) a nor'easter storm on November 10-13, 1999. Wind speed observations from the FRF station and NOAA Buoy 44014 (top), wind direction (middle), and significant wave height, H_s , at the offshore buoy, X6 (bottom). The vertical lines indicate the time period analyzed for each event.

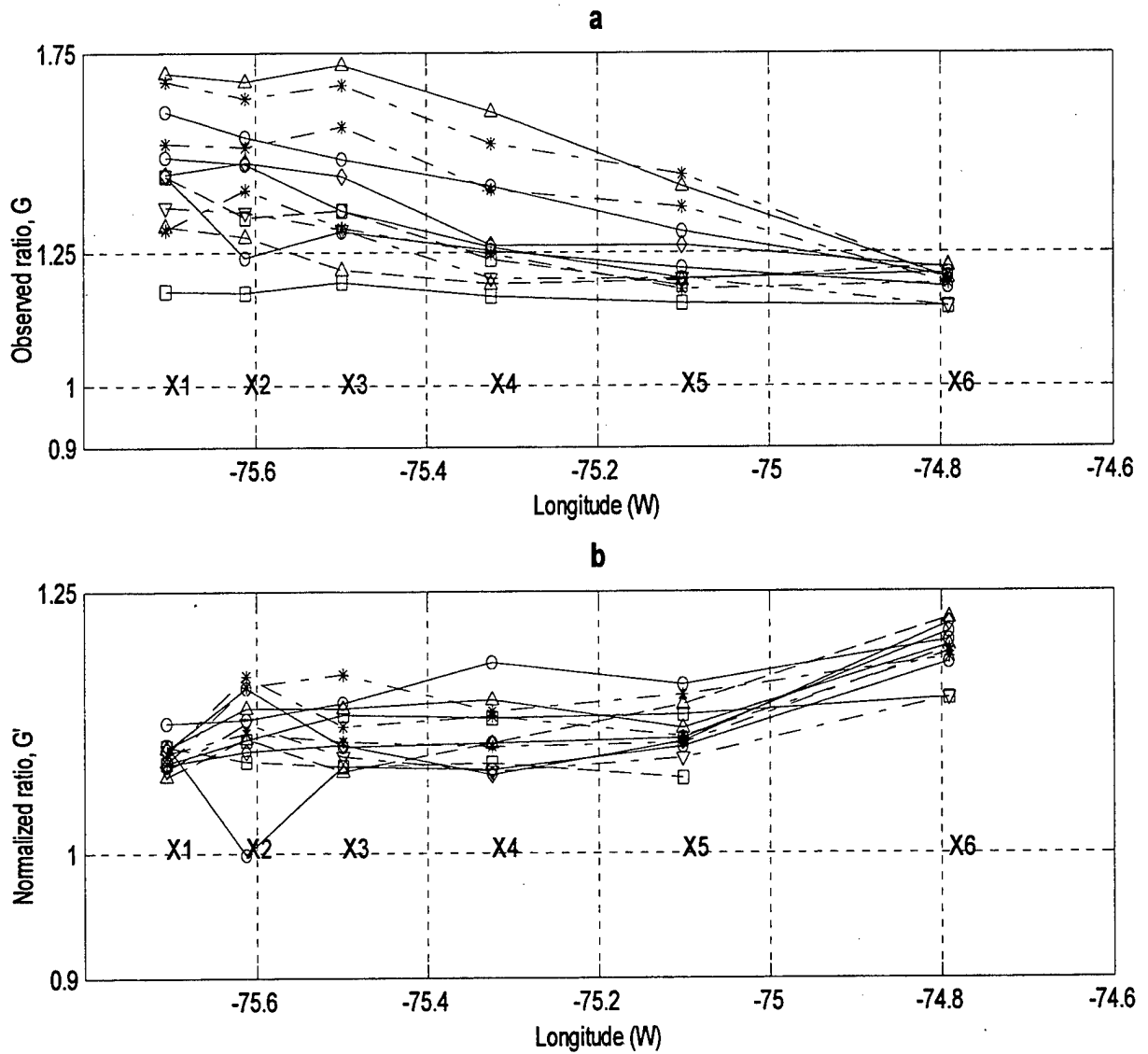


Figure 7. a) The observed ratio, G , and b) the normalized ratio, G' , for each of the 12 swell events listed in Table 2, vs longitude.

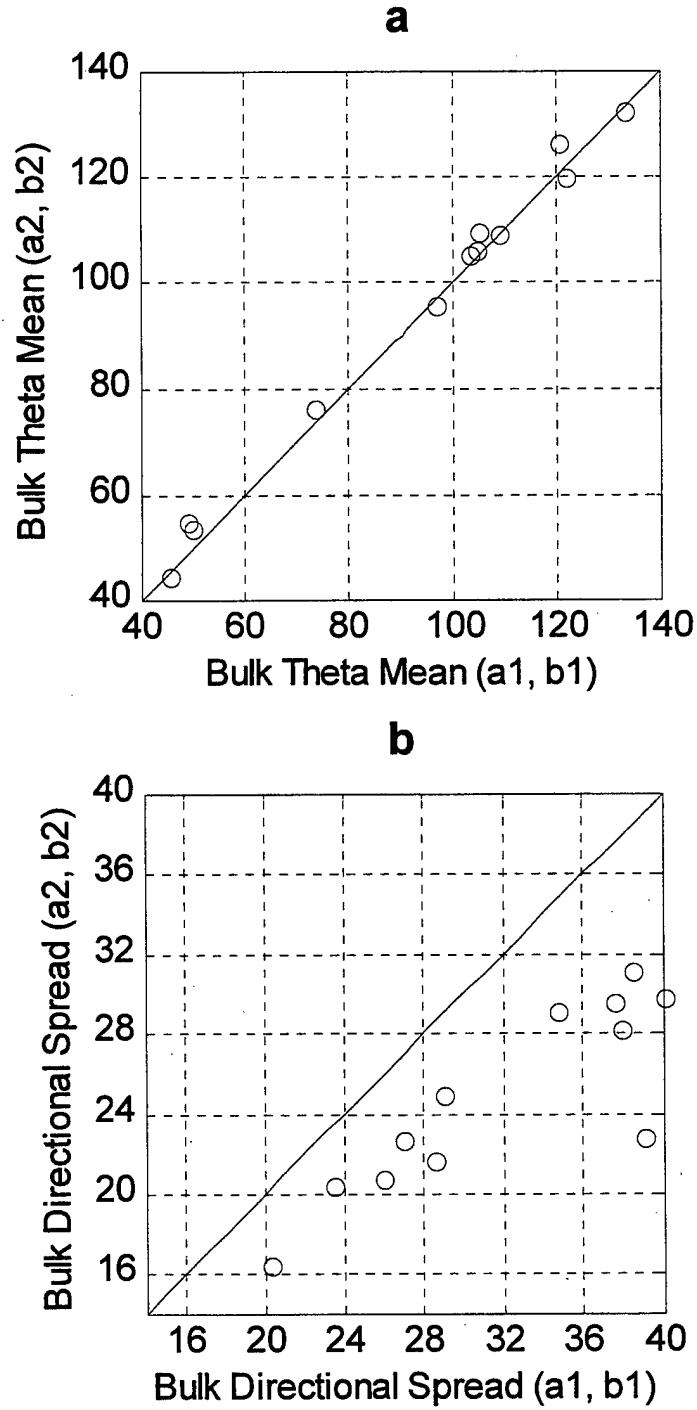


Figure 8. Scatter plots of the second-order (a2, b2) vs first-order (a1, b1) approximations of a) bulk mean propagation direction, θ_{mean} , and b) bulk directional spread, σ_{θ} . Estimates are compared for the 12 case studies listed in Table 2.

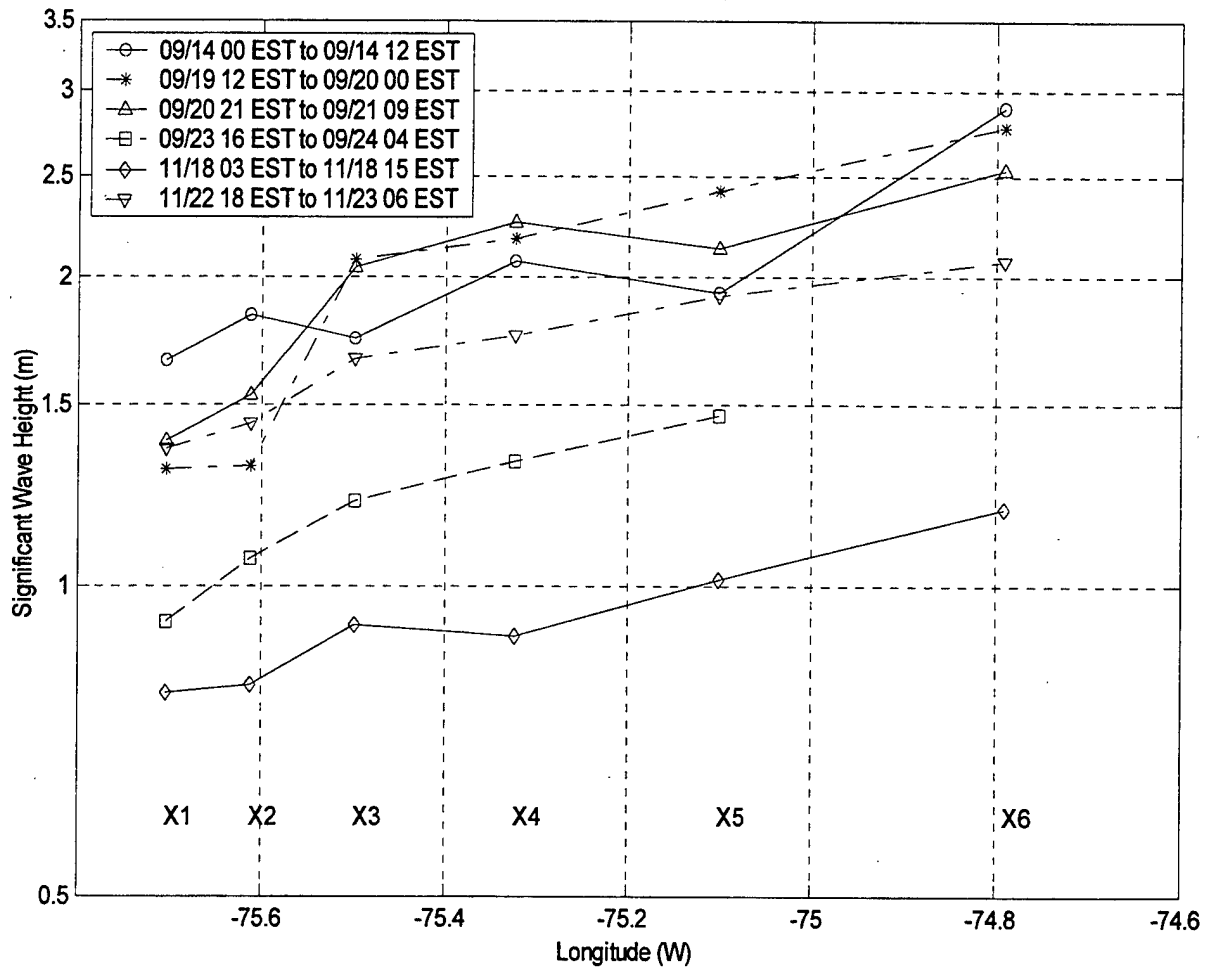


Figure 9. Significant wave heights, H_s , observed in easterly swell cases vs longitude.

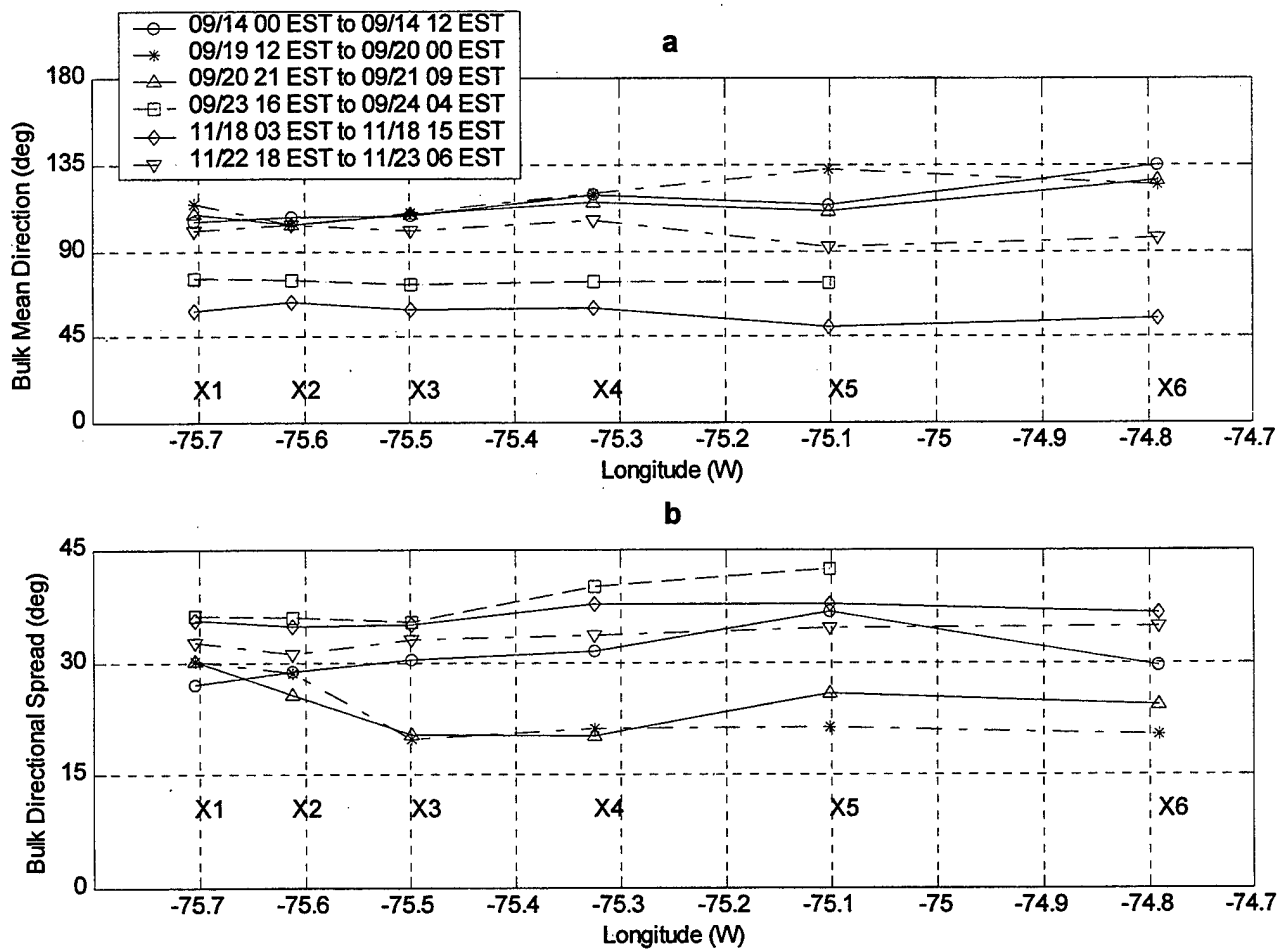


Figure 10. a) Bulk mean direction, θ_{mean} , observed in easterly swell cases vs longitude.
b) Bulk directional spread, σ_{θ} , for the same cases vs longitude.

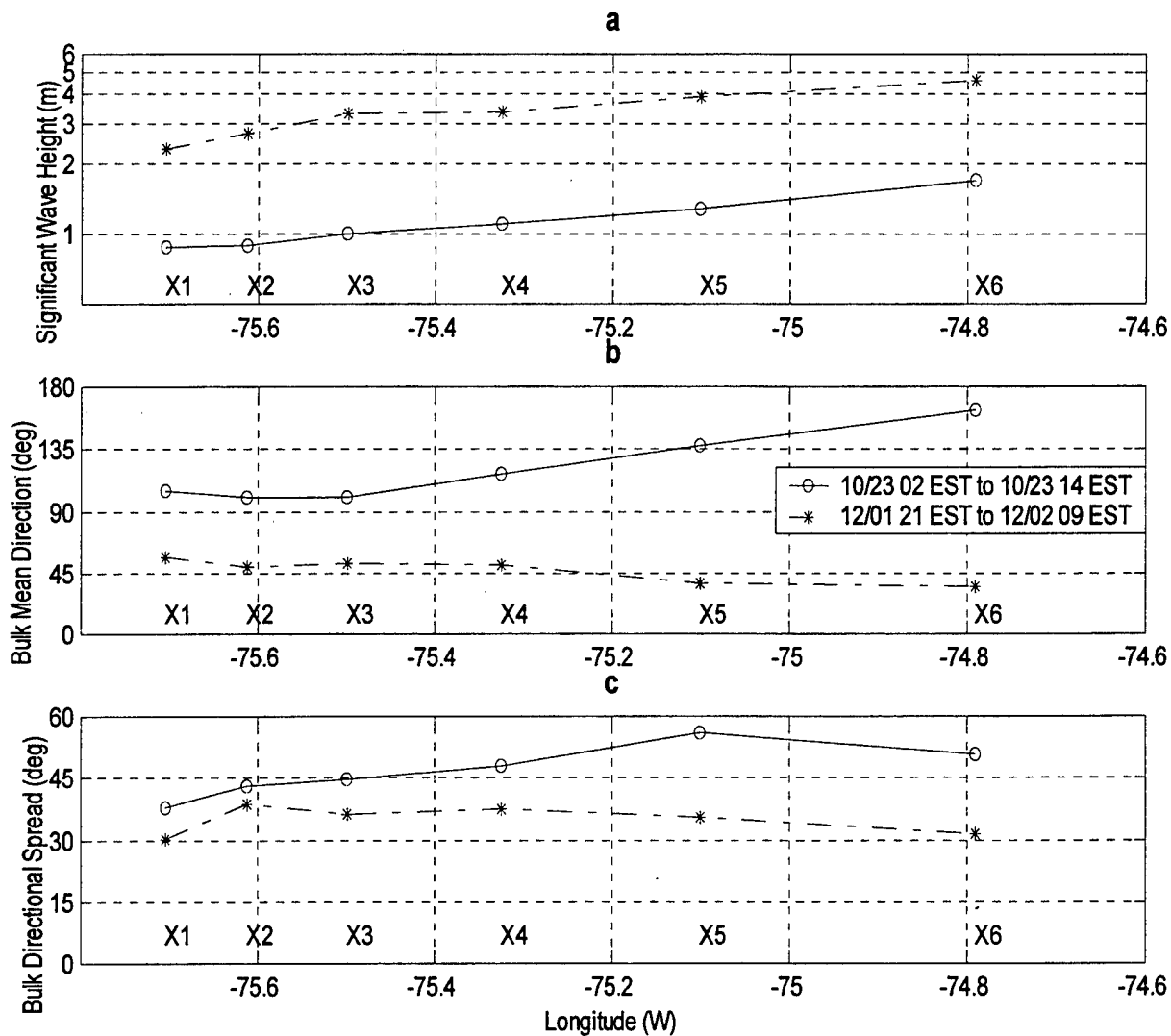


Figure 11. a) H_s , b) θ_{mean} , and c) σ_θ vs longitude for large oblique angle swell cases.

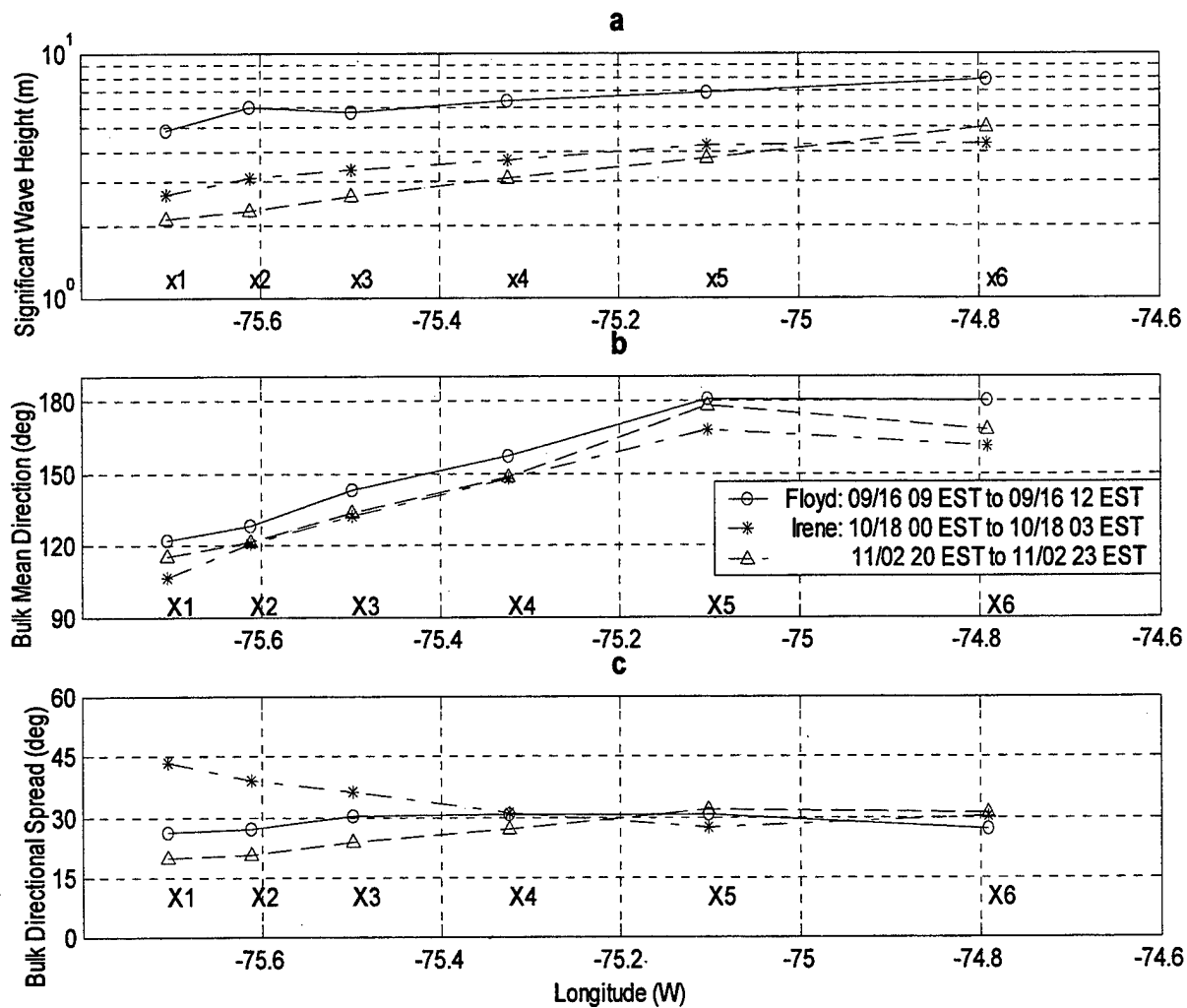


Figure 12. a) H_s , b) θ_{mean} , and c) σ_θ vs longitude for storm waves cases.

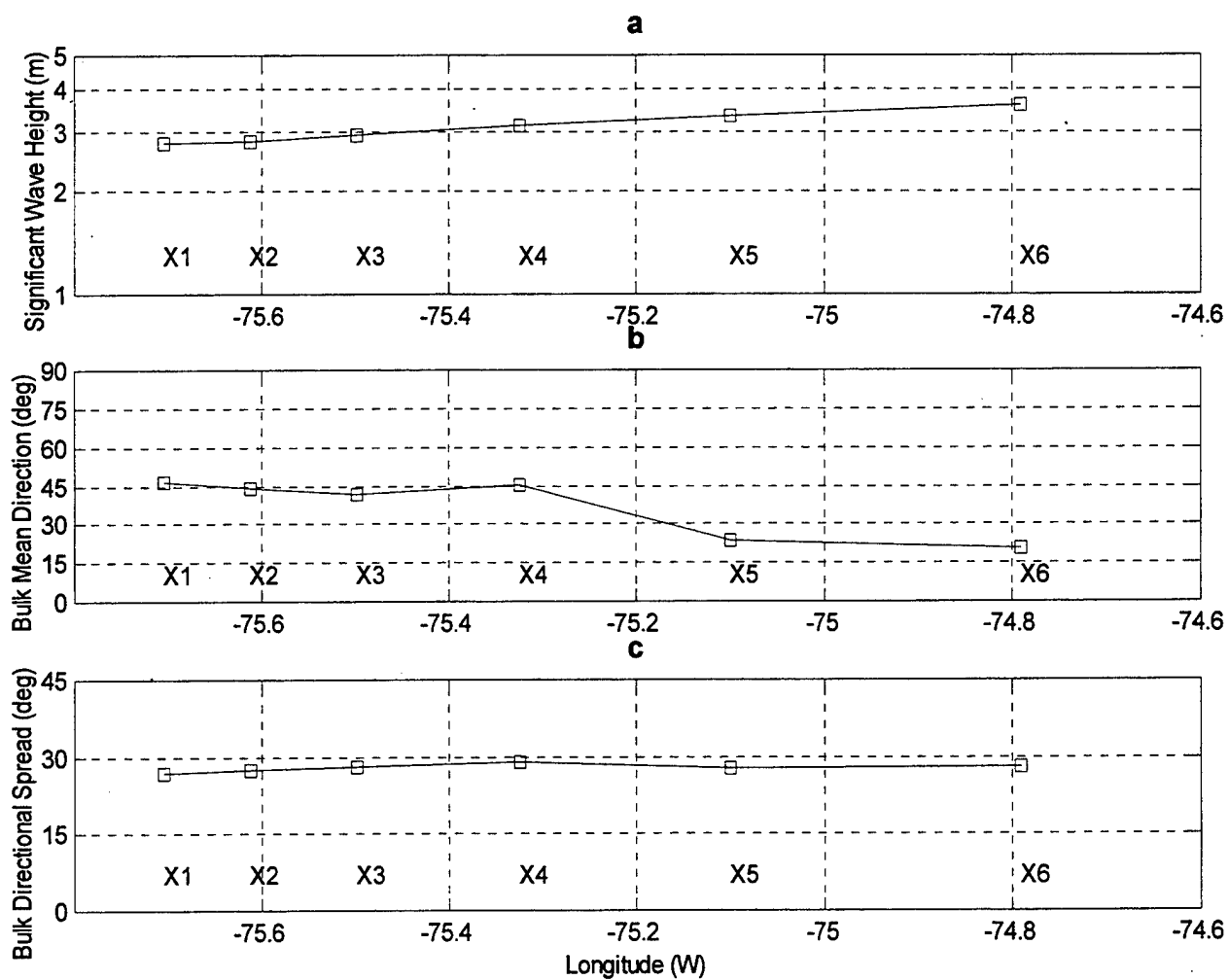


Figure 13. a) H_s , b) θ_{mean} , and c) σ_θ vs longitude for nor'easter swell case.

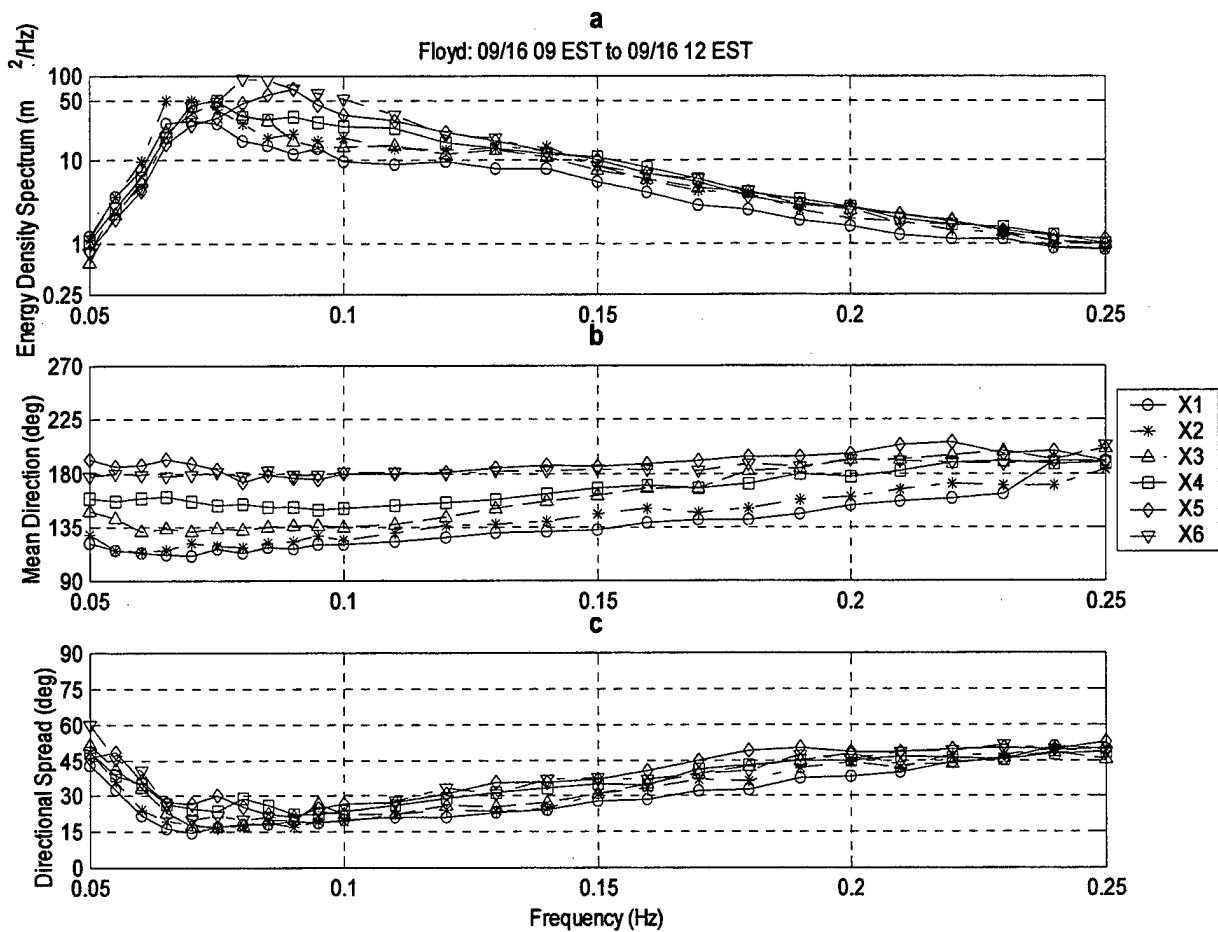


Figure 14. Frequency and direction spectra of all 6 buoys (X1-X6) for Hurricane Floyd. a) The energy density spectra, $E(f)$; b) mean propagation direction, $\theta_{\text{mean}}(f)$; and c) the directional spread, $\sigma_{\theta}(f)$.

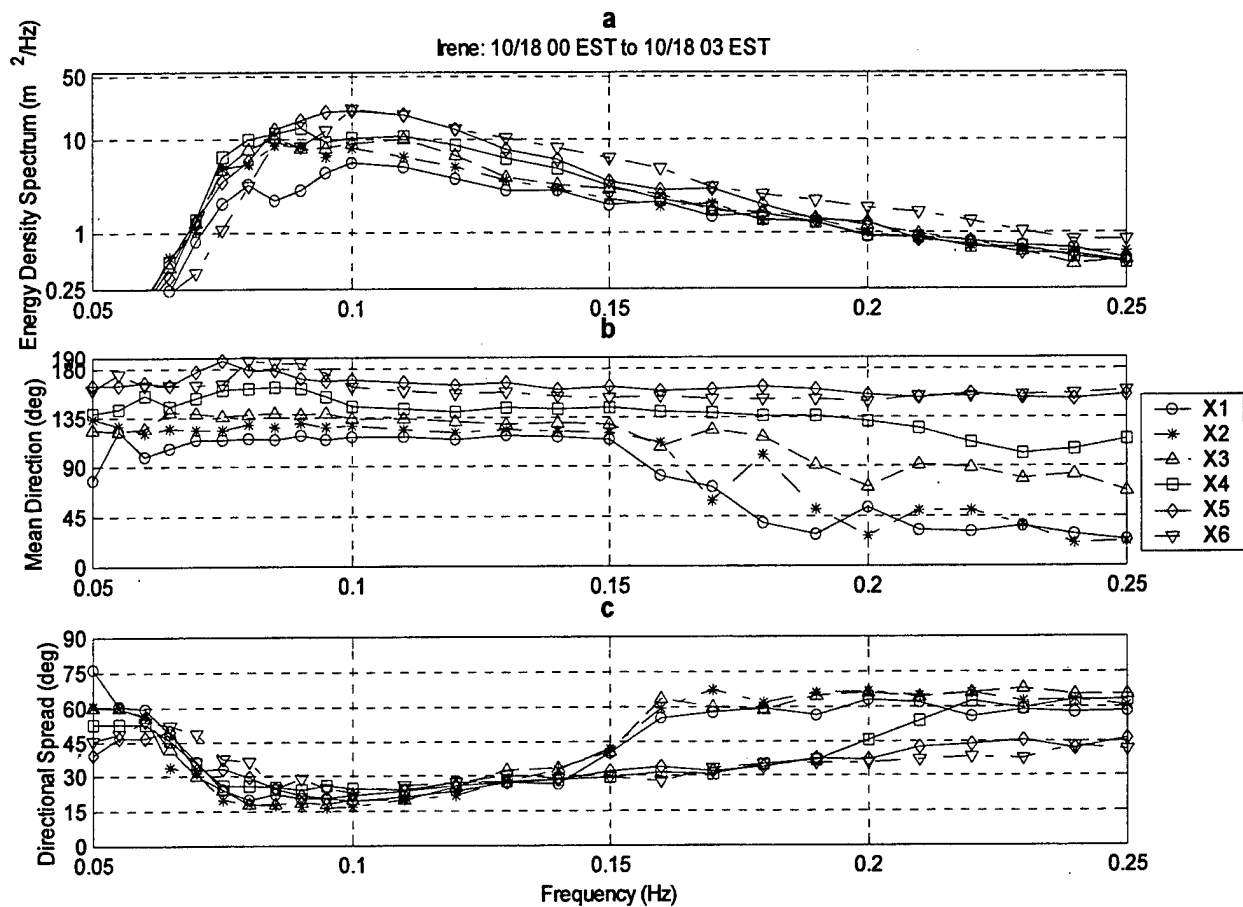


Figure 15. Frequency and direction spectra of all 6 buoys (X1-X6) for Hurricane Irene.
a) The energy density spectra, $E(f)$; b) mean propagation direction, $\theta_{\text{mean}}(f)$; and c) the directional spread, $\sigma_{\theta}(f)$.

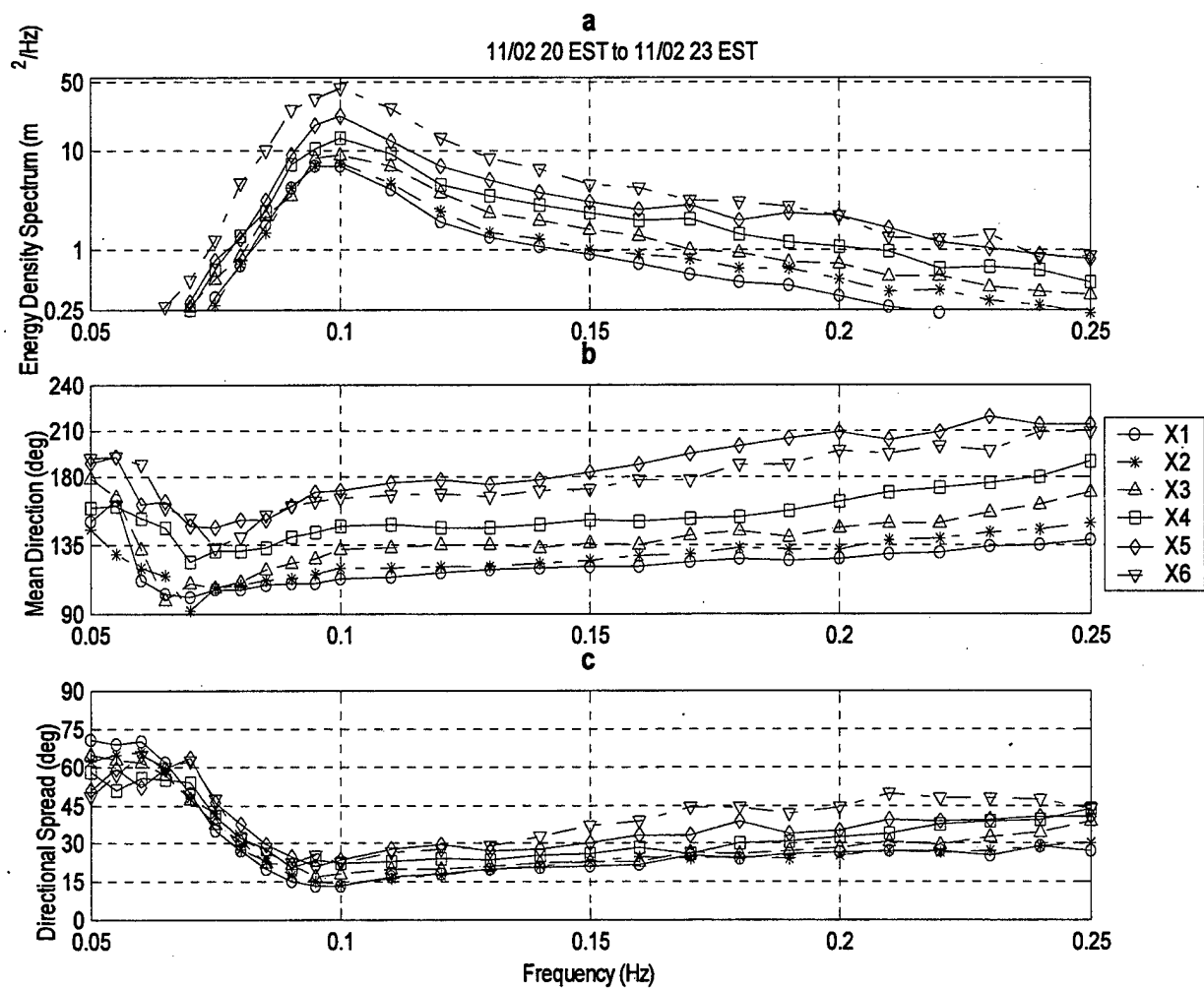


Figure 16. Frequency and direction spectra of all 6 buoys (X1-X6) for the November 2 storm. a) The energy density spectra, $E(f)$; b) mean propagation direction, $\theta_{\text{mean}}(f)$; and c) the directional spread, $\sigma_{\theta}(f)$.

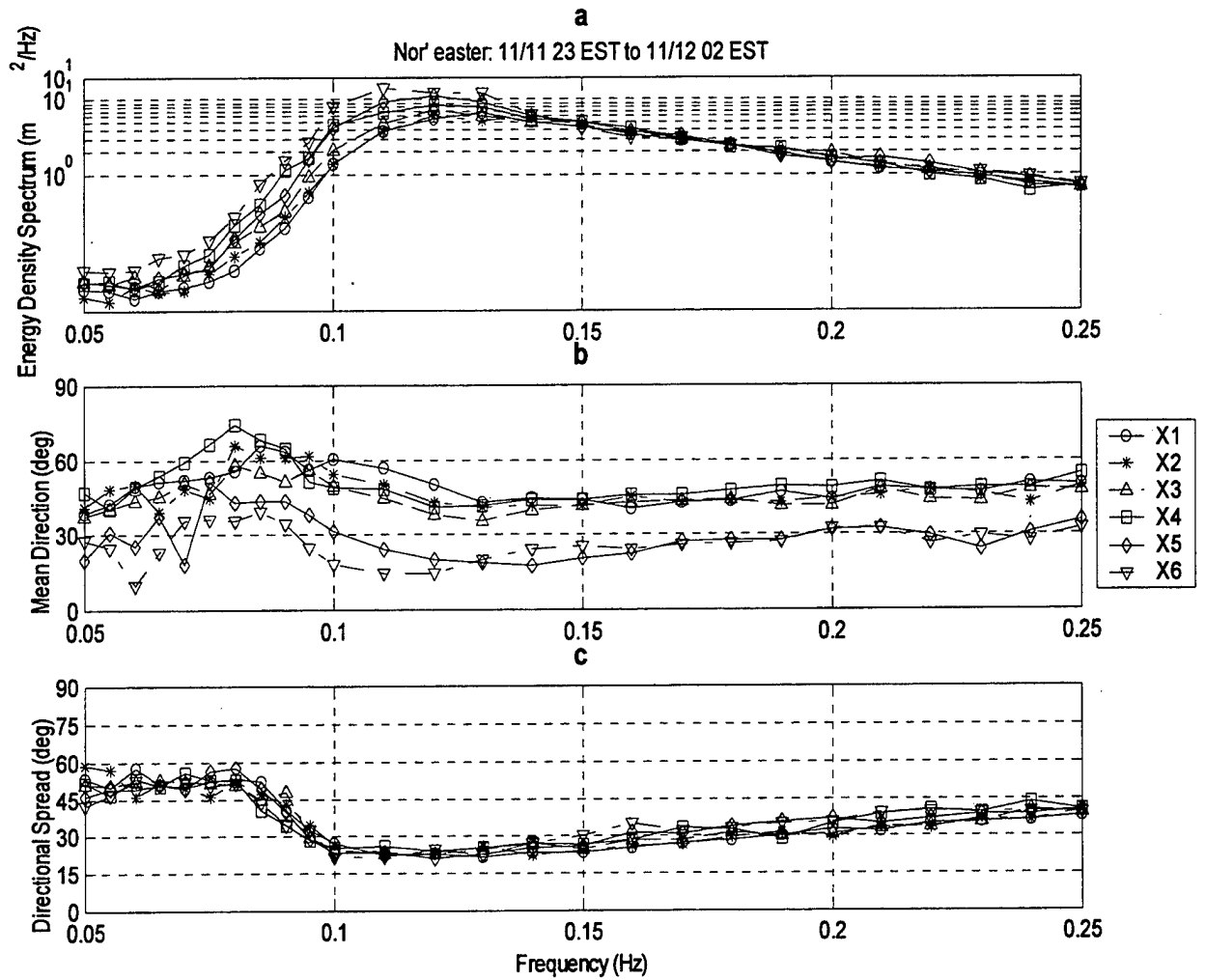


Figure 17. Frequency and direction spectra of all 6 buoys (X1-X6) for the nor'easter case. a) The energy density spectra, $E(f)$; b) mean propagation direction, $\theta_{\text{mean}}(f)$; and c) the directional spread, $\sigma_{\theta}(f)$.

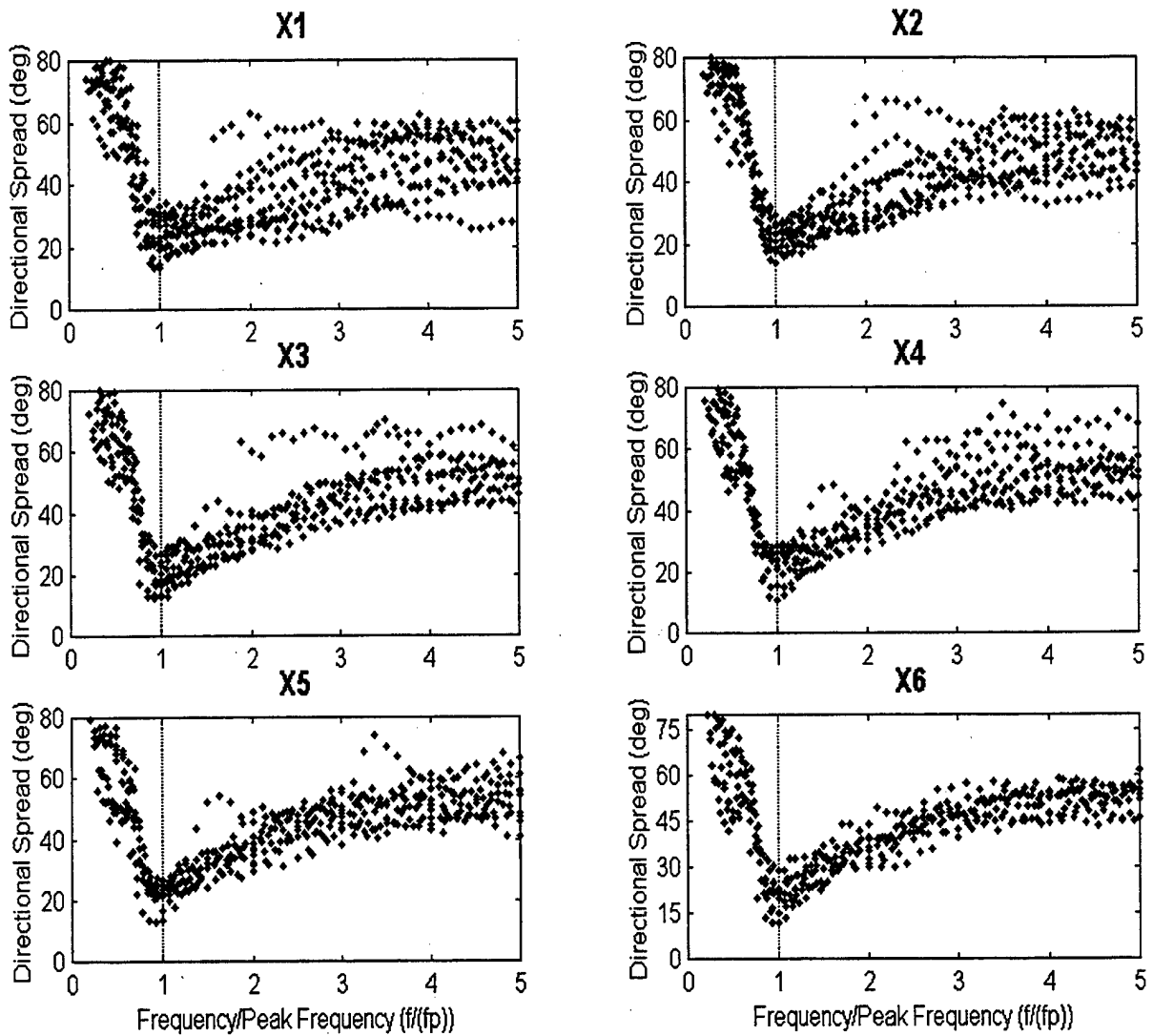


Figure 18. σ_θ estimates of all twelve case studies vs normalized frequency (f/f_p) for each buoy.

THIS PAGE INTENTIONALLY LEFT BLANK

LIST OF REFERENCES

- Datawell bv. (1995). Operation and Service Manual for "Directional Waverider".
Haarlem, the Netherlands.
- Forristall, G. Z., and A. M. Reece, 1985, "Measurements of wave attenuation due to a soft bottom: the SWAMP experiment", *J. Geophys. Res.*, 90, C2, 3367-3380.
- Graber, H.C., M. W. Byman, and W. Rosenthal, 1990, "Numerical simulations of surface wave refraction in the North Sea, Part 1: Kinematics", *Dtsch. Hydrogr. Z.*, 43, 1-18.
- Grant, W. D., and O. S. Madsen, 1982, "Moveable bed roughness in unsteady oscillatory flow", *J. Geophys. Res.*, 87, 469-481.
- Hasselmann, D. E., M. Dunkel, and J. A. Ewing, 1980, "Directional Wave Spectra Observed during JONSWAP 1973", *J. Phys. Oceanogr.*, 10, 1264-1280.
- Hasselmann, K., T. P. Barnett, E. Bouws, H. Carlsson, D. E. Cartwright, K. Enke, J. A. Ewing, H. Gienapp, D. E. Hasselmann, P. Kruseman, A. Meerburg, P. Muller, D. J. Olbers, K. Richter, W. Sell, and H. Walden, 1973, "Measurements of wind wave growth and swell decay during the Joint North Sea Wave Project (JONSWAP)", *Dtsch. Hydrogr. Z. Suppl.* A8(12), 95.
- Herbers, T. H. C., S. Elgar, and R. T. Guza, 1999, "Directional spreading of waves in the nearshore", *J. Geophys. Res.*, 104, C4, 7683-7693.
- Herbers, T. H. C., E. J. Hendrickson, and W. C. O'Reilly, 2000, "Propagation of swell across a wide continental shelf", *J. Geophys. Res.*, (in press).
- Kuik, A. J., G. P. van Vledder, and L. H. Holthuijsen, 1988, "A method for routine analysis of pitch-and-roll buoy data", *J. Phys. Oceanogr.*, 18, 1020-1034.
- Le Méhauté, B., and J. D. Wang, 1982, "Wave spectrum changes on a sloped beach, *J. Waterw., Port, Coastal Ocean Eng.*, 108, 33-47.
- Long, R. B., 1973, "Scattering of surface waves by an irregular bottom", *J. Geophys. Res.*, 78, 7861-7870.
- Long, R. B., 1980, "The statistical evaluation of directional spectrum estimates derived from pitch/roll buoy data", *J. Phys. Oceanogr.*, 10, 944-952.

- Longuet-Higgins, M. S., 1957, "On the transformation of a continuous spectrum by refraction", *Proc. Cam. Phil. Soc.*, 53, 226-229.
- Longuet-Higgins, M. S., D. E. Cartwright, and N. D. Smith, 1963, "Observations of the directional spectrum of sea waves using the motions of a floating buoy", *Ocean Wave Spectra*, pp. 111-136, Prentice-Hall, Englewood Cliffs, N. J.
- Mitsuyasu, H., F. Tasai, T. Suhara, S. Mizuno, M. Ohkusu, T. Honda, and K. Rikiishi, 1975, "Observations of the directional spectrum of ocean waves using a cloverleaf buoy", *J. Phys. Oceanogr.*, 5, 750-760.
- O'Reilly, W. C., and R. T. Guza, 1993, "A comparison of two spectral wave models in the Southern California Bight", *Coastal Engineering* 19, 263-282.
- Munk, W.H., and R. S. Arthur, 1951, "Wave intensity along a refracted ray." Circular 521, Gravity Waves, National Bureau of Standards, 95-108.
- Shemdin, O. H., V. Hsiao, H. E. Carlson, K. Hasselmann, and K. Shulze, 1980, "Mechanisms of wave transformation in finite water depth", *J. Geophys. Res.*, 85, 5012-51018.
- Snodgrass, F. E., G. W. Groves, K. F. Hasselmann, G. R. Miller, W. H. Munk, and W. H. Powers, 1966, "Propagation of ocean swell across the pacific", *Phil. Trans. Roy. Soc. Lond.*, A259, 431-497.
- The WAMDI Group, 1988, "The WAM model-A third generation ocean wave prediction model", *J. Phys. Oceanogr.* 18, 1775-1810.
- Tolman, H. L., 1994, "Wind waves and movable-bed bottom friction", *J. Phys. Oceanogr.*, 24, 994-1009.
- Young, I. R., and R. M. Gorman, 1995, "Measurements of the evolution of ocean wave spectra due to bottom friction", *J. Geophys. Res.*, 100, 10987-11004.

INITIAL DISTRIBUTION LIST

1. Defense Technical Information Center.....2
8725 John J. Kingman Rd., Ste 0944
Ft. Belvoir, VA 22060-6218
2. Dudley Knox Library.....2
Naval Postgraduate School
411 Dyer Rd
Monterey, CA 93943-5101
3. Professor T. H. C. Herbers, Code OC/He.....8
Department of Oceanography
Naval Postgraduate School
Monterey, CA 93943-5121
4. Professor E. B. Thorton, Code OC/Tm.....1
Department of Oceanography
Naval Postgraduate School
Monterey, CA 93943-5121
5. Cynthia Viernes Tinder.....1
1607 Airy Hill Ct Apt C
Crofton, MD 21114
6. Michelle D. Viernes.....1
752 Billow Dr
San Diego, CA 92114